Laser cooling below the Doppler limit by polarization gradients: simple theoretical models

J. Dalibard and C. Cohen-Tannoudji

Collège de France et Laboratoire de Spectroscopie Hertzienne de l'Ecole Normale Supérieure [Laboratoire associé au Centre National de la Recherche Scientifique (LA18) et à l'Université Paris VI], 24, rue Lhomond, F-75231 Paris Cedex 05, France

Received April 3, 1989; accepted June 29, 1989

We present two cooling mechanisms that lead to temperatures well below the Doppler limit. These mechanisms are based on laser polarization gradients and work at low laser power when the optical-pumping time between different ground-state sublevels becomes long. There is then a large time lag between the internal atomic response and the atomic motion, which leads to a large cooling force. In the simple case of one-dimensional molasses, we identify two types of polarization gradient that occur when the two counterpropagating waves have either orthogonal linear polarizations or orthogonal circular polarizations. In the first case, the light shifts of the ground-state Zeeman sublevels are spatially modulated, and optical pumping among them leads to dipole forces and to a Sisyphus effect analogous to the one that occurs in stimulated molasses. In the second case ($\sigma^+-\sigma^-$ configuration), the cooling mechanism is radically different. Even at very low velocity, atomic motion produces a population difference among ground-state sublevels, which gives rise to unbalanced radiation pressures. From semiclassical optical Bloch equations, we derive for the two cases quantitative expressions for friction coefficients and velocity capture ranges. The friction coefficients are shown in both cases to be independent of the laser power, which produces an equilibrium temperature proportional to the laser power. The lowest achievable temperatures then approach the one-photon recoil energy. We briefly outline a full quantum treatment of such a limit.

1. INTRODUCTION

The physical mechanism that underlies the first proposals for laser cooling of free atoms[1] or trapped ions[2] is the Doppler effect. Consider, for example, a free atom moving in a weak standing wave, slightly detuned to the red. Because of the Doppler effect, the counterpropagating wave gets closer to resonance and exerts a stronger radiation pressure on the atom than the copropagating wave. It follows that the atomic velocity is damped, as if the atom were moving in a viscous medium (optical molasses). The velocity capture range Δv of such a process is obviously determined by the natural width Γ of the atomic excited state

$$k\Delta v \sim \Gamma, \tag{1.1}$$

where k is the wave number of the laser wave. On the other hand, by studying the competition between laser cooling and diffusion heating introduced by the random nature of spontaneous emission, one finds that for two-level atoms the lowest temperature T_D that can be achieved by such a method is given by[3,4]

$$k_B T_D = \hbar \frac{\Gamma}{2}. \tag{1.2}$$

T_D is called the Doppler limit. The first experimental demonstrations of optical molasses seemed to agree with such a limit.[5,6]

In 1988, it appeared that such a limit could be overcome. More precise measurements by the National Institute of Standards and Technology Washington group[7] showed that temperatures much lower than T_D, and even approaching the recoil limit T_R given by

$$k_B T_R = \frac{\hbar^2 k^2}{2M}, \tag{1.3}$$

where M is the atomic mass, can be observed on laser-cooled sodium atoms at low laser powers. Such an important result was confirmed soon after by other experiments on sodium[8] and cesium.[9]

A possible explanation for these low temperatures based on new cooling mechanisms resulting from polarization gradients was presented independently by two groups at the last International Conference on Atomic Physics in Paris.[9,10] We summarize below the broad outlines of the argument[11]:

(i) The friction force experienced by an atom moving in a laser wave is due to the fact that the atomic internal state does not follow adiabatically the variations of the laser field resulting from atomic motion.[12,13] Such effects are characterized by a nonadiabaticity parameter ϵ, defined as the ratio between the distance $v\tau$ covered by the atom with a velocity v during its internal relaxation time τ and the laser wavelength $\lambda = 1/k$, which in a standing wave is the characteristic length for the spatial variations of the laser field

$$\epsilon = \frac{v\tau}{\lambda} = kv\tau. \tag{1.4}$$

(ii) For a two-level atom, there is a single internal time, which is the radiative lifetime of the excited state

$$\tau_R = \frac{1}{\Gamma}, \tag{1.5}$$

so that

0740-3224/89/112023-23$02.00

$$\epsilon = kv\tau_R = \frac{kv}{\Gamma}. \tag{1.6}$$

But for atoms, such as alkali atoms, that have several Zeeman sublevels g_m, $g_{m'}$, ...in the ground state g, there is another internal time, which is the optical-pumping time τ_p, characterizing the mean time that it takes for an atom to be transferred by a fluorescence cycle from one sublevel g_m to another $g_{m'}$. We can write

$$\tau_p = \frac{1}{\Gamma'}, \tag{1.7}$$

where Γ' is the mean scattering rate of incident photons and also can be considered the width of the ground state. It follows that for multilevel atoms we must introduce a second nonadiabaticity parameter

$$\epsilon' = kv\tau_p = \frac{kv}{\Gamma'}. \tag{1.8}$$

At low laser power, i.e., when the Rabi frequency Ω is small compared with Γ, we have $\tau_p \gg \tau_R$ and consequently $\Gamma' \ll \Gamma$:

$$\Omega \ll \Gamma \rightarrow \Gamma' \ll \Gamma \rightarrow \epsilon' \gg \epsilon. \tag{1.9}$$

It follows that nonadiabatic effects can appear at velocities ($kv \sim \Gamma'$) much smaller than those required by the usual Doppler-cooling scheme ($kv \sim \Gamma$). This explains why large friction forces can be experienced by very slow atoms.[14]

(iii) The last point concerns the importance of polarization gradients. Long pumping times can give rise to large friction forces only if the internal atomic state in g strongly depends on the position of the atom in the laser wave, so that when the atom is moving there are large changes in its internal state and, consequently, large nonadiabatic effects. By internal atomic state in g, we mean actually the anisotropy in g (usually described in terms of orientation or alignment) that results from the existence of large population differences among the Zeeman sublevels of g or from coherences among these sublevels. Polarization gradients are essential if there are to be important spatial variations of the ground-state anisotropy. For example, if the polarization changes from σ^+ to σ^-, the equilibrium internal state in g changes from a situation in which the atom is pumped in g_m with $m = J_g$ to a situation in which it is pumped in $g_{m'}$ with $m' = -J_g$; if the polarization ϵ is linear and rotates, the atomic alignment in g is parallel to ϵ and rotates with ϵ. By contrast, in the low-power regime considered here [see expression (1.9)], a gradient of light intensity without gradient of polarization would produce only a slight change of the total population in g (which remains close to 1) without any change of the anisotropy in g.[15]

Finally, note that the laser field does not produce only optical pumping between the Zeeman sublevels of g; it also induces light shifts $\Delta_{m'}$ that can vary from one sublevel to the other. Another consequence of polarization gradients is that the various Zeeman sublevels in g have not only a population but also a light-shifted energy and a wave function that can vary in space.

The purpose of this paper is to analyze in detail the physical mechanisms of these new cooling schemes by polarization gradients and to present a few simple theoretical models for one-dimensional (1-D) molasses, permitting a quantitative calculation of the new friction force and of the equilibrium temperature. Our treatment will be limited here to a J_g to $J_e = J_g + 1$ transition, neglecting all other possible hyperfine levels of the optical transition.

We first introduce, for a 1-D molasses, two types of polarization gradient (see Section 2). In the first case, which occurs with two counterpropagating waves with opposite (σ^+ and σ^-) circular polarizations, the polarization vector rotates when one moves along the standing wave, but it keeps the same ellipticity. In the second case, which occurs, for example, with two counterpropagating waves with orthogonal linear polarizations, the ellipticity of the laser polarization varies in space, but the principal axis of polarization remain fixed. The basic difference between these two situations is that the second configuration can give rise to dipole or gradient forces but the first one cannot.

Section 3 is devoted to a physical discussion of the cooling mechanisms associated with these two types of polarization gradient; they are shown to be quite different. In the configuration with orthogonal linear polarizations, hereafter denoted as the lin $\perp$ lin configuration, the light shifts of the various Zeeman sublevels of g oscillate in space, and optical pumping among these sublevels provides a cooling mechanism analogous to the Sisyphus effect occurring in high-intensity stimulated molasses[16,17]: The atom is always climbing potential hills. In the σ^+–σ^- configuration, the combined effect of the rotation of the polarization and of optical pumping and light shifts produces a highly sensitive motion-induced population difference among the Zeeman sublevels of g (defined with respect to the axis of the standing wave) and, consequently, a large imbalance between the radiation pressures of the two counterpropagating waves.

In Sections 4 and 5 some quantitative results for 1-D molasses and simple atomic transitions are presented. In Section 4 the case of a transition $J_g = 1/2 \leftrightarrow J_e = 3/2$ is considered for an atom moving in the lin $\perp$ lin configuration, whereas in Section 5 the case of a $J_g = 1 \leftrightarrow J_e = 2$ transition is considered for an atom moving in the σ^+–σ^- configuration. In Sections 4 and 5, atomic motion is treated semiclassically: the spatial extent of the atomic wave packet is neglected and the force at a given point in the laser wave is calculated. Since the new cooling mechanisms work at low power, the calculations are limited to the perturbative regime ($\Omega \ll \Gamma$), where it is possible to derive from optical Bloch equations a subset of equations that involve only the populations and Zeeman coherences in the atomic ground state g. In both configurations, analytical or numerical solutions of Bloch equations are derived that are then used to analyze the velocity dependence of the mean radiative force. Quantitative results are derived for the friction coefficient, the velocity capture range, and the equilibrium temperature, which is shown to be proportional to the laser power Ω^2.

When the laser power is low enough, the equilibrium temperature approaches the recoil limit T_R. It is then clear that the semiclassical treatment breaks down, since the de Broglie wavelength of an atom with $T = T_R$ is equal to the laser wavelength. At the end of Section 5, a full quantum treatment is presented of the cooling process in the σ^+–σ^- configuration for a simplified atomic-level scheme. Such a treatment is similar to the one used in the analysis of other cooling schemes allowing temperatures of the order of or below T_R to be reached.[18,19] We show that the velocity

distribution curves exhibit a very narrow structure around $v = 0$, with a width of a few recoil velocities, in agreement with the semiclassical predictions.

2. TWO TYPES OF POLARIZATION GRADIENT IN A ONE-DIMENSIONAL MOLASSES

In this section, we consider two laser plane waves with the same frequency ω_L that propagate along opposite directions on the Oz axis and we study how the polarization vector of the total electric field varies when one moves along Oz. Let $\mathcal{E}_0$ and $\mathcal{E}_0'$ be the amplitudes of the two waves and ϵ and ϵ' be their polarizations. The total electric field $\mathbf{E}(z, t)$ in z at time t can be written as

$$\mathbf{E}(z, t) = \mathcal{E}^+(z)\exp(-i\omega_L t) + \text{c.c.}, \tag{2.1}$$

where the positive-frequency component $\mathcal{E}^+(z)$ is given by

$$\mathcal{E}^+(z) = \mathcal{E}_0\epsilon e^{ikz} + \mathcal{E}_0'\epsilon' e^{-ikz}. \tag{2.2}$$

By a convenient choice of the origin on the Oz axis, we can always take $\mathcal{E}_0$ and $\mathcal{E}_0'$ real.

A. The σ^+-σ^- Configuration—Pure Rotation of Polarization

We consider first the simple case in which

$$\epsilon = \epsilon_+ = -\frac{1}{\sqrt{2}}(\epsilon_x + i\epsilon_y), \tag{2.3a}$$

$$\epsilon' = \epsilon_- = \frac{1}{\sqrt{2}}(\epsilon_x - i\epsilon_y). \tag{2.3b}$$

The two waves have opposite circular polarizations, σ^- for the wave propagating toward $z < 0$ and σ^+ for the other wave.

Inserting Eqs. (2.3) into Eq. (2.2), we get

$$\mathcal{E}^+(z) = \frac{1}{\sqrt{2}}(\mathcal{E}_0' - \mathcal{E}_0)\epsilon_X - \frac{i}{\sqrt{2}}(\mathcal{E}_0' + \mathcal{E}_0)\epsilon_Y, \tag{2.4}$$

where

$$\epsilon_X = \epsilon_x \cos kz - \epsilon_y \sin kz, \tag{2.5a}$$

$$\epsilon_Y = \epsilon_x \sin kz + \epsilon_y \cos kz. \tag{2.5b}$$

The total electric field in z is the superposition of two fields in quadrature, with amplitudes $(\mathcal{E}_0' - \mathcal{E}_0)/\sqrt{2}$ and $(\mathcal{E}_0' + \mathcal{E}_0)/\sqrt{2}$ and polarized along two orthogonal directions ϵ_X and ϵ_Y deduced from ϵ_x and ϵ_y by a rotation of angle $\varphi = -kz$ around Oz. We conclude that the polarization of the total electric field is elliptical and keeps the same ellipticity, $(\mathcal{E}_0' - \mathcal{E}_0)/(\mathcal{E}_0' + \mathcal{E}_0)$ for all z. When one moves along Oz, the axes of the ellipse just rotate around Oz by an angle $\varphi = -kz$. As expected, the periodicity along z is determined by the laser wavelength $\lambda = 2\pi/k$.

Previous analysis shows that, for a σ^+-σ^- configuration, we have a pure rotation of polarization along Oz. By pure we mean that the polarization rotates but keeps the same ellipticity. One can show that the σ^+-σ^- configuration is the only one that gives such a result.

In the simple case in which the two counterpropagating waves σ^+ and σ^- have the same amplitude $\mathcal{E}_0 = \mathcal{E}_0'$, the total electric field is, according to expression (3.4) below, linearly polarized along ϵ_Y. For $z = 0$, ϵ_Y coincides with ϵ_y. When one moves along Oz, ϵ_Y rotates, and its extremity forms a helix with a pitch λ [Fig. 1(a)].

B. The lin ⊥ lin Configuration—Gradient of Ellipticity

We suppose now that the two counterpropagating waves have orthogonal linear polarizations

$$\epsilon = \epsilon_x, \tag{2.6a}$$

$$\epsilon' = \epsilon_y. \tag{2.6b}$$

If we suppose, in addition, that the two waves have equal amplitudes, we get from Eqs. (2.2) and (2.6)

$$\mathcal{E}^+(z) = \mathcal{E}_0\sqrt{2}\left(\cos kz\,\frac{\epsilon_x + \epsilon_y}{\sqrt{2}} - i\sin kz\,\frac{\epsilon_y - \epsilon_x}{\sqrt{2}}\right). \tag{2.7}$$

The total electric field is the superposition of two fields in quadrature, with amplitudes $\mathcal{E}_0\sqrt{2}\cos kz$ and $\mathcal{E}_0\sqrt{2}\sin kz$, and polarized along two fixed orthogonal vectors $(\epsilon_y \pm \epsilon_x)/\sqrt{2}$ parallel to the two bisectrices of $\mathbf{e}_x$ and $\mathbf{e}_y$. It is clear that the ellipticity changes now when one moves along Oz. From Eq. (2.7) we see that the polarization is linear along $\epsilon_1 = (\epsilon_x + \epsilon_y)/\sqrt{2}$ in $z = 0$, circular (σ^-) in $z = \lambda/8$, linear along $\epsilon_2 = (\epsilon_x - \epsilon_y)/\sqrt{2}$ in $z = \lambda/4$, circular (σ^+) in $z = 3\lambda/8$, is linear along $-\epsilon_1$ in $z = \lambda/2$, and so on... [Fig. 1(b)].

If the two amplitudes $\mathcal{E}_0$ and $\mathcal{E}_0'$ are not equal, we still have the superposition of two fields in quadrature; however, now they are polarized along two fixed but nonorthogonal directions. For $\mathcal{E}_0 = \mathcal{E}_0'$ the nature of the polarization of the total field changes along Oz. Such a result generally holds; i.e., for all configurations other than the σ^+-σ^- one, there are gradients of ellipticity when one moves along Oz (excluding, of course, the case when both waves have the same polarization).

C. Connection with Dipole Forces and Redistribution

The two laser configurations of Figs. 1(a) and 1(b) differ radically with regard to dipole forces. Suppose that we have in z an atom with several Zeeman sublevels in the ground state g. For example, we consider the simple case of a $J_g = 1/2 \leftrightarrow J_e = 3/2$ transition for which there are two Zeeman sublevels, $g_{-1/2}$ and $g_{+1/2}$, in g and four Zeeman sublevels in e. It is easy to see that the z dependence of the light shifts of the two ground-state sublevels is quite different for the two laser configurations of Figs. 1(a) and 1(b). For the σ^+-σ^- configuration, the laser polarization is always linear, and the laser intensity is the same for all z. It follows that the two light-shifted energies are equal and do not vary with z [Fig. 1(c)]. On the other hand, since the Clebsch–Gordan coefficients of the various transitions $g_m \leftrightarrow e_{m'}$ are not the same, and since the nature of the polarization changes with z, one can easily show (see Subsection 3.A.1) that the two light-shifted energies oscillate with z for the lin ⊥ lin configuration [Fig. 1(d)]: the $g_{1/2}$ sublevel has the largest shift for a σ^+ polarization the $g_{-1/2}$ sublevel has the largest shift for a σ^- polarization, whereas both sublevels are equally shifted for a linear polarization.

The striking difference between the z dependences of the light-shifted energies represented in Figs. 1(c) and 1(d)

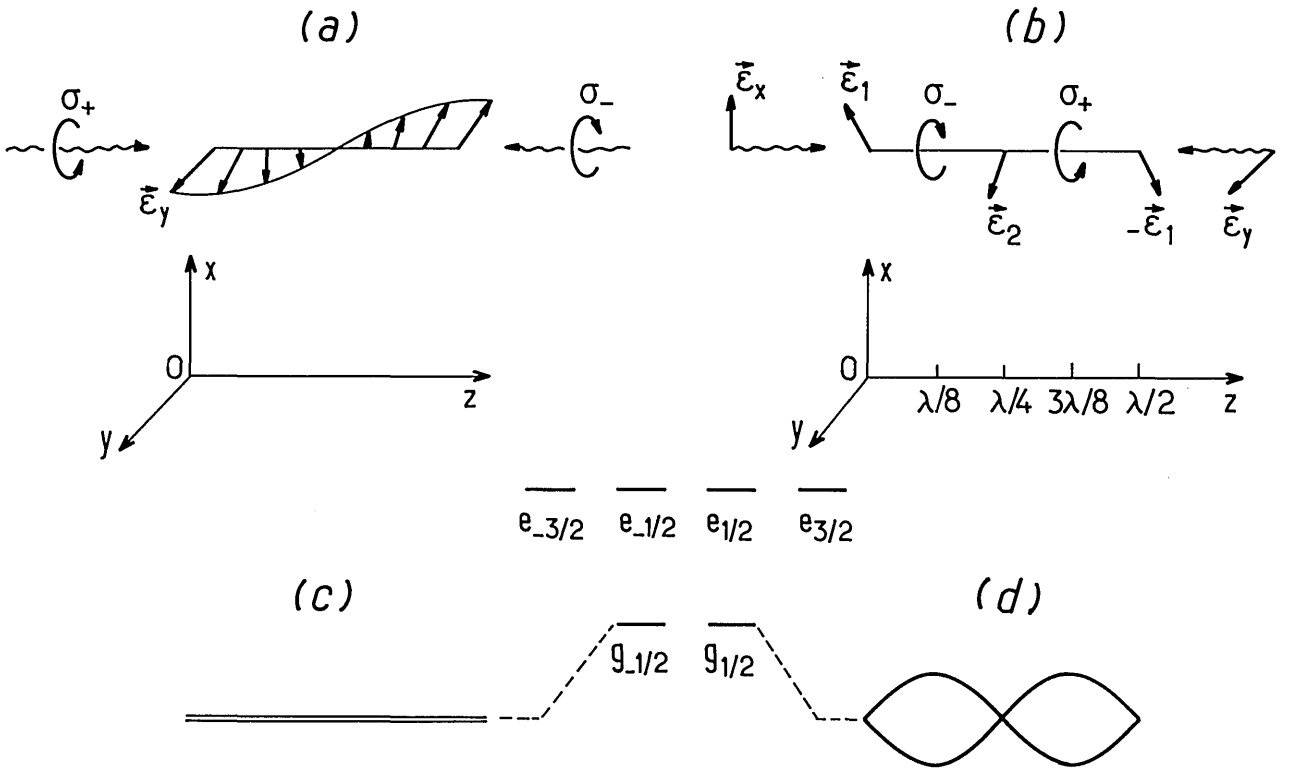

Fig. 1. The two types of polarization gradient in a 1-D molasses and the corresponding light-shifted ground-state sublevels for a $J_g = 1/2 \leftrightarrow J_e = 3/2$ atomic transition. (a) σ^+–σ^- configuration: two counterpropagating waves, σ^+ and σ^- polarized, create a linear polarization that rotates in space. (b) lin ⊥ lin configuration: The two counterpropagating waves have orthogonal linear polarizations. The resulting polarization now has an ellipticity that varies in space: for $z = 0$ linear polarization along $\epsilon_1 = (\epsilon_x + \epsilon_y)/\sqrt{2}$; for $z = \lambda/8$ σ^- polarization; for $z = \lambda/4$ linear polarization along $\epsilon_2 = (\epsilon_x - \epsilon_y)/\sqrt{2}$; for $z = 3\lambda/8$ σ^+ circular polarization.... (c) Light-shifted ground-state sublevels for the σ^+–σ^- configuration: The light-shifted energies do not vary with z. (d) Light-shifted ground-state sublevels for the lin ⊥ lin configuration: The light-shifted energies oscillate in space with a period $\lambda/2$.

means that there are dipole or gradient forces in the configuration of Fig. 1(b), whereas such forces do not exist in the configuration of Fig. 1(a). We use here the interpretation of dipole forces in terms of gradients of dressed-state energies.[16] Another equivalent interpretation can be given in terms of redistribution of photons between the two counterpropagating waves, when the atom absorbs a photon from one wave and transfers it via stimulated emission into the opposite wave.[12,20] It is obvious that conservation of angular momentum prevents such a redistribution from occurring in the configuration of Fig. 1(a).[21] After it absorbs a σ^+ photon, the atom is put into $e_{+1/2}$ or $e_{+3/2}$, and there are no σ^- transitions starting from these levels and that could be used for the stimulated emission of a σ^- photon. For more complex situations, such as for a $J_g = 1 \leftrightarrow J_e = 2$ transition (see Fig. 5 below), redistribution is not completely forbidden but is limited to a finite number of processes. Suppose, for example, that the atom is initially in g_{-1}. When it absorbs a σ^+ photon, it jumps to e_0. Then, by stimulated emission of a σ^- photon, it falls to g_{+1}, from where it can be reexcited to e_{+2} by absorption of a σ^+ photon. However, once in e_{+2}, the atom can no longer make a stimulated emission in the σ^- wave, since no σ^- transition starts from e_{+2}. We thus have in this case a limited redistribution, and one can show that, as in Fig. 1(c), the light-shifted energies in the ground state do not vary with z (see Subsection 3.B.1). The situation is completely different for the configuration of Fig. 1(b). Then, each σ^+ or σ^- transition can be excited by both linear polarizations ϵ_x and ϵ_y, and an infinite number of redistribution processes between the two counterpropagating waves can take place via the same transition $g_m \leftrightarrow e_{m+1}$ or e_{m-1}. This is why the light-shifted energies vary with z in Fig. 1(d).

Finally, let us note that, at first sight, one would expect dipole forces to be inefficient in the weak-intensity limit considered in this paper since, in general, they become large only at high intensity, when the splitting among dressed states is large compared with the natural width Γ.[16] Actually, here we consider an atom that has several sublevels in the ground state. The light-shift splitting between the two oscillating levels of Fig. 1(d) can be large compared with the width Γ' of these ground-state sublevels. Furthermore, we show in Subsection 3.A.2 that for a moving atom, even with weak dipole forces, the combination of long pumping times and dipole forces can produce a highly efficient new cooling mechanism.

3. PHYSICAL ANALYSIS OF TWO NEW COOLING MECHANISMS

In this section, we consider a multilevel atom moving in a laser configuration exhibiting a polarization gradient. We begin (Subsection 3.A) by analyzing the lin ⊥ lin configuration of Fig. 1(b), and we show how optical pumping between the two oscillating levels of Fig. 1(d) can give rise to a new cooling mechanism analogous to the Sisyphus effect occurring in stimulated molasses.[16,17] Such an effect cannot exist

for the configuration of Fig. 1(a) since the energy levels of Fig. 1(c) are flat. We show in Subsection 3.B that there is a new cooling mechanism associated with the $\sigma^+-\sigma^-$ configuration, but it has a completely different physical interpretation.

The emphasis in this section will be on physical ideas. A more quantitative analysis, based on optical Bloch equations, is presented in the following sections.

A. Multilevel Atom Moving in a Gradient of Ellipticity

The laser configuration is the lin $\perp$ lin configuration of Fig. 1(b). As in Subsection 2.C, we take a $J_g = 1/2 \leftrightarrow J_e = 3/2$ transition. The Clebsch–Gordan coefficients of the various transitions $g_m \leftrightarrow e_{m'}$ are indicated in Fig. 2. The square of these coefficients give the transition probabilities of the corresponding transitions.

1. *Equilibrium Internal State for an Atom at Rest*

We first show that, for an atom at rest in z, the energies and the populations of the two ground-state sublevels depend on z.

Suppose, for example, that $z = \lambda/8$ so that the polarization is σ^- [Fig. 1(b)]. The atom is optically pumped in $g_{-1/2}$ so that the steady-state populations of $g_{-1/2}$ and $g_{1/2}$ are equal to 1 and 0, respectively. We must also note that, since the σ_- transition starting from $g_{-1/2}$ is three times as intense as the σ_- transition starting from $g_{1/2}$, the light shift Δ_-' of $g_{-1/2}$ is three times larger (in modulus) than the light-shift Δ_+' of $g_{1/2}$. We assume here that, as usual in Doppler-cooling experiments, the detuning

$$\delta = \omega_L - \omega_A \tag{3.1}$$

between the laser frequency ω_L and the atomic frequency ω_A is negative so that both light shifts are negative.

If the atom is at $z = 3\lambda/8$, where the polarization is σ^+ [Fig. 1(b)], the previous conclusions are reversed. The populations of $g_{-1/2}$ and $g_{1/2}$ are equal to 0 and 1, respectively, because the atom is now optically pumped into $g_{1/2}$. Both light shifts are still negative, but we now have $\Delta_+' = 3\Delta_-'$.

Finally, if the atom is in a place where the polarization is linear, for example, if $z = 0, \lambda/4, \lambda/2 \ldots$ [Fig. 1(b)], symmetry considerations show that both sublevels are equally populated and undergo the same (negative) light shift equal to 2/3 times the maximum light shift occurring for a σ^+ or σ^- polarization.

All these results are summarized in Fig. 3, which shows as a function of z the light-shifted energies of the two ground-state sublevels of an atom at rest in z. The sizes of the black circles represented on each sublevel are proportional to the steady-state population of this sublevel. It clearly appears in Fig. 3 that the energies of the ground-state sublevels oscillate in space with a spatial period $\lambda/2$ and that the lowest-energy sublevel is also the most populated one.

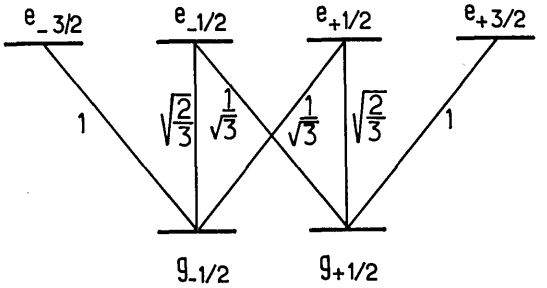

Fig. 2. Atomic level scheme and Clebsh–Gordan coefficients for a $J_g = 1/2 \leftrightarrow J_e = 3/2$ transition.

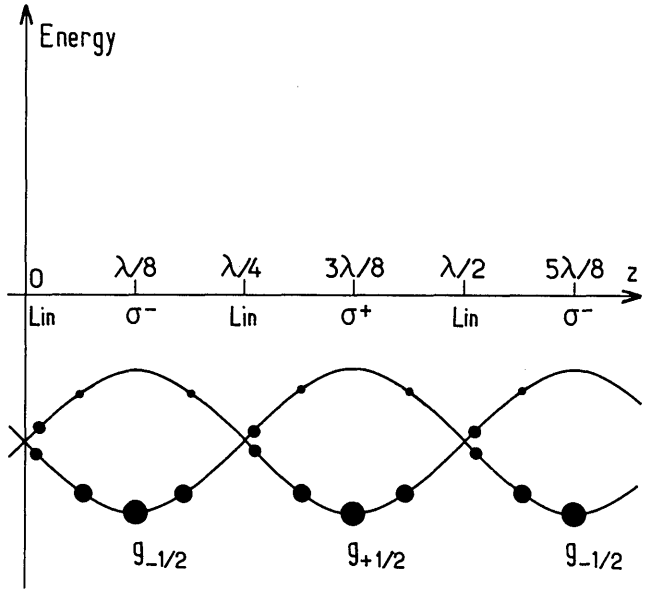

Fig. 3. Light-shifted energies and steady-state populations (represented by filled circles) for a $J_g = 1/2$ ground state in the lin $\perp$ lin configuration and for negative detuning. The lowest sublevel, having the largest negative light shift, is also the most populated one.

2. *Sisyphus Effect for a Moving Atom*

We suppose now that the atom is moving along Oz, and we try to understand how its velocity can be damped. The key point is that optical pumping between the two ground-state sublevels takes a finite time τ_p. Suppose that the atom starts from the bottom of a potential valley, for example, at $z = \lambda/8$ (see Fig. 4), and that it moves to the right. If the velocity v is such that the atom travels over a distance of the order of $\lambda/4$ during τ_p, the atom will on average remain on the same sublevel, climb the potential hill, and reach the top of this hill before being optically pumped to the other sublevel, i.e., to the bottom of the next potential valley at $z = 3\lambda/8$. From there, the same sequence can be repeated (see the solid lines in Fig. 4). It thus appears that, because of the time lag τ_p, the atom is always climbing potential hills, transforming part of its kinetic energy into potential energy. Here we have an atomic example of the Sisyphus myth that is quite analogous to the cooling effect that occurs in stimulated molasses and discussed in Ref. 16. Note, however, that the effect discussed in this paper appears at much lower intensities than in Ref. 16 since it involves two ground-state sublevels with spatially modulated light shifts Δ' much smaller than Γ; on the contrary, in Ref. 16 the modulation of the dressed-state energies is much larger than Γ.

3. *Mechanism of Energy Dissipation and Order of Magnitude of the Friction Coefficient*

The previous physical picture clearly shows how the atomic kinetic energy is converted into potential energy: The atom climbs a potential hill. In the same way as for the usual dipole forces, one can also understand how the atomic momentum changes during the climbing. There is a corre-

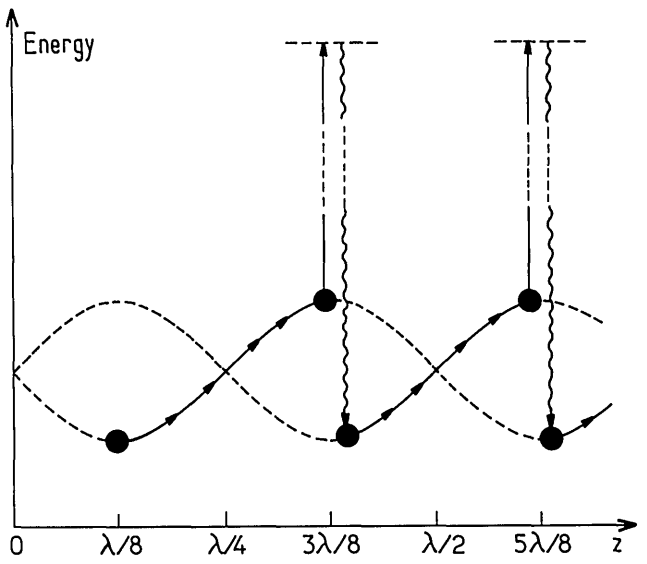

Fig. 4. Atomic Sisyphus effect in the lin ⊥ lin configuration. Because of the time lag τ_p due to optical pumping, the atom sees on the average more uphill parts than downhill ones. The velocity of the atom represented here is such that $v\tau_p \sim \lambda$, in which case the atom travels overs λ in a relaxation time τ_p. The cooling force is then close to its maximal value.

sponding change of momentum of the laser field because of a coherent redistribution of photons between the two counterpropagating waves. Photons are absorbed from one wave and transferred by stimulated emission to the other wave. All these processes are conservative and could occur in both ways. The atom could slide down a potential hill and transform its potential energy into kinetic energy. Optical pumping is the mechanism of energy dissipation essential for introducing irreversibility into the process and for producing cooling. We see from Fig. 4 that when the atom reaches the top of the hill, there is a great probability that it will absorb a laser photon $\hbar\omega_L$ and emit a fluorescence photon, blue-shifted by an amount corresponding to the light-shift splitting between the two ground-state sublevels. The gain of potential energy at the expense of kinetic energy is dissipated by spontaneous Raman anti-Stokes photons that carry away the excess of energy. Here also we find a mechanism quite analogous to the one occurring in stimulated molasses.[16] Note, however, that the energy dissipated here is much smaller, since it corresponds to the light shift of the ground state at low laser power.

From the previous discussion, we can derive an order of magnitude of the friction coefficient α appearing in the low-velocity expression

$$F = -\alpha v \tag{3.2}$$

of the friction force. It is clear in Fig. 4 that the maximum value of the friction force occurs when $v\tau_p \sim \lambda/4$, i.e., when

$$kv \sim \Gamma', \tag{3.3}$$

where $\Gamma' = 1/\tau_p$. For this value of v, the energy dissipated during τ_p is of the order of $-\hbar\Delta'$ (since $\Delta' < 0$), so the energy dissipated per unit time is

$$\frac{dW}{dt} \sim \frac{-\hbar\Delta'}{\tau_p} = -\hbar\Delta'\Gamma'. \tag{3.4}$$

On the other hand, we can also calculate dW/dt from F:

$$\frac{dW}{dt} \sim -Fv. \tag{3.5}$$

Since we evaluate only orders of magnitude, we can keep the linear expression (3.2) of F, even when v is given by expression (3.3), so that

$$\frac{dW}{dt} \sim -\alpha v^2. \tag{3.6}$$

Equating expressions (3.4) and (3.6) and using expression (3.3) of v, we finally obtain

$$\alpha \sim -\hbar k^2 \frac{\Delta'}{\Gamma'}. \tag{3.7}$$

Since all the previous considerations are restricted to the low-intensity limit (we want to have Γ', $|\Delta'| \ll \Gamma$), Δ' and Γ' are both proportional to the laser intensity. It then follows from expression (3.7) that the friction coefficient of this new cooling mechanism is independent of the laser power at low power. This clearly distinguishes this new friction force from the usual one occurring in Doppler cooling, which is linear in laser power. We can still transform expression (3.7) by using the expressions of Γ' and Δ' at low power ($\Omega \ll \Gamma$). Assuming, in addition, a large detuning ($|\delta| \gg \Gamma$) in order to have in the ground-state light shifts larger than the level widths, we get

$$\Gamma' \sim \Omega^2\Gamma/\delta^2, \tag{3.8a}$$

$$\Delta' \sim \Omega^2/\delta, \tag{3.8b}$$

so that

$$\alpha \sim -\hbar k^2 \frac{\delta}{\Gamma}. \tag{3.9}$$

Note, finally, that the friction coefficient [expression (3.7) or (3.9)] is large, and even larger (since $|\delta| \gg \Gamma$) than the optimal friction coefficient for the usual Doppler cooling, which is of the order of $\hbar k^2$.[3,4] One must not forget, however, that the velocity capture range of this new friction force, which is given by expression (3.3), is much smaller than the velocity capture range for Doppler cooling (given by $kv \sim \Gamma$). One can also understand why α is so large, despite the fact that the size $\hbar|\Delta'|$ of the potential hills of Fig. 4 is so small. We see in expression (3.7) that $\hbar|\Delta'|$ is divided by Γ', which is also very small since the optical-pumping time is very long. In other words, the weakness of dipole forces is compensated for by the length of the optical-pumping times.

B. Multilevel Atom Moving in a Rotating Laser Polarization

The laser configuration is now the σ^+-σ^- laser configuration of Fig. 1(a) for which the laser polarization remains linear and rotates around Oz, forming an helix with a pitch λ. As shown in Fig. 1(c), the light shifts of the ground-state sublevels remain constant when the atom moves along Oz, and there is no possibility of a Sisyphus effect. Such a result is easily extended to all values of J_g. If J_g were larger than 1/2, we would have in Fig. 1(c) several horizontal lines instead of a single one, since sublevels g_m with different values of $|m|$ have different light shifts and since there are several possible values for $|m|$ when $J_g > 1/2$.

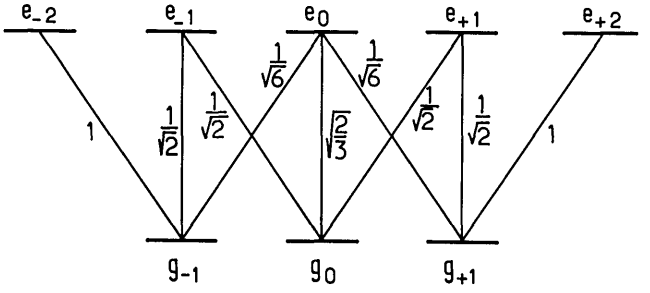

Fig. 5. Atomic level scheme and Clebsh–Gordan coefficients for a $J_g = 1 \leftrightarrow J_e = 2$ transition.

In this subsection we describe a new cooling mechanism that works in the σ^+–σ^- laser configuration for atoms with $J_g \geqslant 1$ and is quite different from the one discussed in Subsection 3.A. We show that, even at very low velocity, there is an atomic orientation along Oz that appears in the ground state as a result of atomic motion. Because of this highly sensitive motion-induced atomic orientation, the two counterpropagating waves are absorbed with different efficiencies, which gives rise to unbalanced radiation pressures and consequently to a net friction force. We consider here the simplest possible atomic transition for such a scheme, the transition $J_g = 1 \leftrightarrow J_e = 2$ (see Fig. 5).

1. Equilibrium Internal State for an Atom at Rest

We suppose first that the atom is at rest in $z = 0$. If we take the quantization axis along the local polarization, which is ϵ_y at $z = 0$ [see Fig. 1(a)], and if we note that $|g_{-1}\rangle_y$, $|g_0\rangle_y$, $|g_1\rangle_y$, the eigenstates of J_y (**J**: angular momentum), we see that optical pumping, with a π polarization along Oy, will concentrate atoms in $|g_0\rangle_y$, since the optical-pumping rate $|g_{-1}\rangle_y \rightarrow |g_0\rangle_y$ proportional to $(1/\sqrt{2})^2(1/\sqrt{2})^2 = 1/4$ is greater than the rate $|g_0\rangle_y \rightarrow |g_{-1}\rangle_y$ proportional to $(\sqrt{2/3})^2(1/\sqrt{6})^2 = 1/9$. The steady-state populations of $|g_0\rangle_y$, $|g_{-1}\rangle_y$, and $|g_{+1}\rangle_y$ are equal to 9/17, 4/17, and 4/17, respectively.

We must also note that, since the π transition starting from $|g_0\rangle_y$ is 4/3 as more intense as the two π transitions starting from $|g_{\pm 1}\rangle_y$, both sublevels $|g_{\pm 1}\rangle_y$ undergo the same light shift Δ_1', smaller (in modulus) than the light-shift Δ_0' of $|g_0\rangle_y$

$$\Delta_0' = \tfrac{4}{3}\Delta_1'. \tag{3.10}$$

As in the previous subsection, we take a red detuning so that Δ_0' and Δ_1' are both negative. Figure 6 represents the light-shifted ground-state sublevels in $z = 0$ with their steady-state populations.

For subsequent discussions, it will be useful to analyze briefly the spectrum of the fluorescence light emitted by an atom at rest in $z = 0$. We suppose that the laser power is very weak ($\Omega \ll \Gamma$) and that the detuning is large ($|\delta| \gg \Gamma$). To the lowest order in Ω^2/δ^2, we find first a Rayleigh line at ω_L corresponding to fluorescence cycles where the atom starts and ends in the same ground-state sublevel. We also have a Raman–Stokes line at $\omega_L + (\Delta_0'/4)$ (remember that $\Delta_0' < 0$), corresponding to cycles where the atom starts from $|g_0\rangle_y$ and ends in $|g_{+1}\rangle_y$ or $|g_{-1}\rangle_y$, and a Raman–anti-Stokes line at $\omega_L - (\Delta_0'/4)$, corresponding to the inverse processes where the atom starts from $|g_{+1}\rangle_y$ or $|g_{-1}\rangle_y$ and ends in $|g_0\rangle_y$. In steady state, the populations of the various ground-state sublevels adjust themselves to values such that the mean number of Stokes processes from $|g_0\rangle_y$ to $|g_{-1}\rangle_y$ balances the mean number of anti-Stokes processes from $|g_{-1}\rangle_y$ to $|g_0\rangle_y$. It is thus clear that in steady state, the mean number of photons emitted per unit time at $\omega_L + (\Delta_0'/4)$ and $\omega_L - (\Delta_0'/4)$ will be equal, giving rise to a symmetrical fluorescence spectrum.

So far, we have considered only an atom at rest in $z = 0$. If the atom is in a different location but still at rest, the same calculations can be repeated, giving rise to the same values for the light shifts (since the laser intensity does not change with z) and to the same steady-state populations. We must note, however, that the wave functions vary in space, since the light-shifted Zeeman sublevels are the eigenstates of the component of **J** along the rotating laser polarization ϵ_Y. It follows that, when the atom moves along Oz, nonadiabatic couplings can appear among the various Zeeman sublevels undergoing different light shifts.

2. Moving Atom—Transformation to a Moving Rotating Frame

The atom is now moving with a velocity v along Oz:

$$z = vt. \tag{3.11}$$

In its rest frame, which moves with the same velocity v, the atom sees a linear polarization ϵ_Y, which rotates around Oz in the plane xOy, making an angle with Oy [see Fig. 1(a) and Eq. (2.5b)]

$$\varphi = -kz = -kvt. \tag{3.12}$$

It is then convenient to introduce, in the atomic rest frame, a rotating frame such that in this moving rotating frame the laser polarization keeps a fixed direction. Of course, Larmor's theorem tells us that, in this moving rotating frame, an inertial field will appear as a result of the rotation. This inertial field looks like a (fictitious) magnetic field parallel to the rotation axis Oz and has an amplitude such that the corresponding Larmor frequency is equal to the rotation speed kv. More precisely, one can show (see Appendix A) that the new Hamiltonian, which governs the

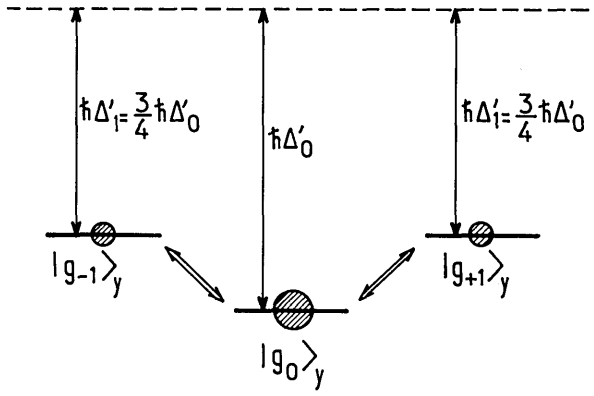

Fig. 6. Light-shifted ground-state sublevels of a $J_g = 1 \leftrightarrow J_e = 2$ transition in the σ^+–σ^- configuration. The quantization axis Oy is chosen along the resulting linear laser polarization. The steady-state populations of these states (4/17, 9/17, 4/17) are represented by the filled circles. The double arrows represent couplings between Zeeman sublevels owing to the transformation to the moving rotating frame.

atomic evolution after the unitary transformation to the moving rotating frame, contains, in addition to a coupling term with a fixed-polarization laser field, an extra inertial term resulting from the rotation and equal to

$$V_{\text{rot}} = kvJ_z. \tag{3.13}$$

If we compare the new Hamiltonian in the moving rotating frame with the Hamiltonian for an atom at rest in $z = 0$ considered in Subsection 3.B.1 we see that all the new effects that are due to atomic motion in a rotating laser polarization must come from the inertial term [Eq. (3.13)]. Since J_z has nonzero matrix elements among the eigenstates of J_y, this inertial term introduces couplings proportional to kv between $|g_0\rangle_y$ and $|g_{\pm 1}\rangle_y$ (double arrows in Fig. 6). These couplings are sometimes called nonadiabatic since they vanish when v tends to 0. We show in the next subsection how they can give rise to an atomic orientation in the ground state that is parallel to Oz and sensitive to kv.

3. Motion-Induced Orientation in the Atomic Ground State

In order to get a clear insight into the modifications introduced by the inertial term [Eq. (3.13)] and also to understand the energy exchanges between the atom and the laser field, it is important to determine first what the new energy levels are in the ground state as well as the new steady-state density matrix in such an energy basis. To simplify the calculations, we assume here that the light shift $|\Delta'|$ is much larger than Γ', so that the energy splitting between the ground-state energy levels is much larger than their widths:

$$\Gamma' \ll |\Delta'|. \tag{3.14a}$$

We also suppose that

$$kv \ll |\Delta'|, \tag{3.14b}$$

which permits a perturbative treatment of the effect of V_{rot}. Quantitative calculations, not restricted by conditions such as Eqs. (3.14) and therefore valid for any velocity, are presented in Section 5.

First, consider the level $|g_0\rangle_y$ in Fig. 6. The perturbation kvJ_z that has no diagonal element in $|g_0\rangle_y$ shifts this level only to second order in kv/Δ'. More important is the modification of the wave function. The state $|g_0\rangle_y$ is contaminated by $|g_1\rangle_y$ and $|g_{-1}\rangle_y$ to first order in kv/Δ', becoming the perturbed state $\overline{|g_0\rangle_y}$. Since we know the matrix elements of J_z in the basis $\{|g_m\rangle_y\}$ of eigenstates of J_y (see Appendix A), we get from first-order perturbation theory

$$\overline{|g_0\rangle_y} = |g_0\rangle_y + \frac{kv}{\sqrt{2}(\Delta_0' - \Delta_1')}|g_{+1}\rangle_y + \frac{kv}{\sqrt{2}(\Delta_0' - \Delta_1')}|g_{-1}\rangle_y. \tag{3.15}$$

Since the matrix elements of J_z in the manifold $\{|g_{+1}\rangle_y, |g_{-1}\rangle_y\}$ are zero, the energies of $|g_{\pm 1}\rangle_y$ are not changed to first order in kv/Δ', while their wave functions become

$$\overline{|g_{+1}\rangle_y} = |g_{+1}\rangle_y + \frac{kv}{\sqrt{2}(\Delta_1' - \Delta_0')}|g_0\rangle_y, \tag{3.16a}$$

$$\overline{|g_{-1}\rangle_y} = |g_{-1}\rangle_y + \frac{kv}{\sqrt{2}(\Delta_1' - \Delta_0')}|g_0\rangle_y. \tag{3.16b}$$

We now study the steady-state density matrix in the energy basis $\{\overline{|g_m\rangle_y}\}$. Since we know the effect of optical pumping in the $\{|g_m\rangle_y\}$ basis and since Eqs. (3.15) and (3.16) give the new states in terms of the old ones, it is possible to show (see Appendix A) that, if we neglect terms of order $(kv/\Delta')^2$, $(kv/\Delta')(\Gamma'/\Delta')$ or higher, the steady-state density matrix ρ_{st} is diagonal in the $\{\overline{|g_m\rangle_y}\}$ basis and has the same diagonal elements as those calculated in Subsection 3.C.1:

$$\overline{{}_y\langle g_0|}\rho_{\text{st}}\overline{|g_0\rangle_y} = 9/17, \tag{3.17a}$$

$$\overline{{}_y\langle g_{+1}|}\rho_{\text{st}}\overline{|g_{+1}\rangle_y} = \overline{{}_y\langle g_{-1}|}\rho_{\text{st}}\overline{|g_{-1}\rangle_y} = 4/17. \tag{3.17b}$$

To sum up, provided that we change from the $\{|g_m\rangle_y\}$ basis to the $\{\overline{|g_m\rangle_y}\}$ basis, the energies and populations of the ground-state sublevels are the same as in Subsection 3.B.1. To first order in kv/Δ' and to zeroth order in Γ'/Δ', the modifications introduced by atomic motion concern only the wave functions.

Now, the important point is that in the perturbed states $\{\overline{|g_m\rangle_y}\}$ the populations of the two eigenstates $|g_{+1}\rangle_z$ and $|g_{-1}\rangle_z$ of J_z are not equal, as they are in $|g_m\rangle_y$. To demonstrate this result, we calculate the average value of J_z in $\overline{|g_m\rangle_y}$, which is proportional to this population difference. From Eqs (3.15) and (3.16), we get

$$\overline{{}_y\langle g_0|}J_z\overline{|g_0\rangle_y} = \frac{2\hbar kv}{\Delta_0' - \Delta_1'}, \tag{3.18a}$$

$$\overline{{}_y\langle g_{+1}|}J_z\overline{|g_{+1}\rangle_y} = \overline{{}_y\langle g_{-1}|}J_z\overline{|g_{-1}\rangle_y} = \frac{\hbar kv}{\Delta_1' - \Delta_0'}. \tag{3.18b}$$

Weighting these values by the populations [Eqs. (3.17)] of the corresponding levels and summing over m, one finds for the steady-state value of J_z that

$$\langle J_z\rangle_{\text{st}} = \frac{2\hbar kv}{\Delta_0' - \Delta_1'}\left(\frac{9}{17} - \frac{2}{17} - \frac{2}{17}\right) = \frac{40}{17}\frac{\hbar kv}{\Delta_0'}, \tag{3.19}$$

where we have used Eqs. (3.10). $\langle J_z\rangle_{\text{st}}$ is a motion-induced atomic orientation in the ground state. Thus we have shown that, when the atom moves along Oz in a rotating laser polarization, the two eigenstates $|g_{\pm 1}\rangle_z$ of J_z have different steady-state populations. Noting Π_{+1} and Π_{-1} for these populations and using $\langle J_z\rangle_{\text{st}} = \hbar(\Pi_{+1} - \Pi_{-1})$, we get from Eq. (3.19)

$$\Pi_{+1} - \Pi_{-1} = \frac{40}{17}\frac{kv}{\Delta_0'}. \tag{3.20}$$

Such a result is in quantitative agreement with the more detailed calculations in Section 5.

Suppose that the atom moves toward $z > 0$, i.e., that $v > 0$. Since we have chosen a red detuning ($\delta < 0$), Δ' is negative. It follows from Eq. (3.20) that $|g_{-1}\rangle_z$ is more populated than $|g_{+1}\rangle_z$:

$$v > 0, \delta < 0 \rightarrow \Pi_{-1} > \Pi_{+1}. \tag{3.21}$$

We show in the next subsection how this motion-induced population difference can give rise to a new much more efficient friction mechanism than the one used in Doppler cooling.

4. Remarks

(i) We saw in Subsection 3.C.2 that the problem studied here is formally equivalent to the problem of an atom at rest,

interacting with a laser field linearly polarized along Oy and submitted to a static magnetic field $\mathbf{B}_0$ along Oz, with an amplitude such that the Larmor frequency in $\mathbf{B}_0$ is equal to kv. Changing v is equivalent to changing $|\mathbf{B}_0|$; such a formulation of the problem allows us to establish a connection between the effects studied in this paper and other well-known effects that were previously observed in optical-pumping experiments. It is well known, for example, that the application of a static field $\mathbf{B}_0$ in a direction different from the symmetry axis of the laser polarization can give rise to very narrow structures in the variations with $|\mathbf{B}_0|$ of the light absorbed or emitted. Examples of such structures are zero-field level-crossing resonances and Hanle resonances in atomic ground states.[22,23] These resonances have a narrow width ΔB_0 such that the Larmor frequency in ΔB_0 is equal to the width Γ' of the ground state, which can be very small at low power.

Actually, the problem studied here is a little more complicated than a pure Hanle effect in the ground state since the laser beam not only introduces an atomic alignment along Oy ($\langle 3J_y^2-\mathbf{J}^2\rangle$ differs from zero) but also produces light shifts of the $|g_m\rangle_y$ states, which have the same symmetry as the Stark shifts that would be produced by a fictitious static electric field $\mathbf{E}_0$ parallel to Oy. In the absence of $\mathbf{B}_0$, the alignment $\langle 3J_y^2-\mathbf{J}^2\rangle$ produced by optical pumping does not precess around $\mathbf{E}_0$, which has the same symmetry axis. When $\mathbf{B}_0$ is applied this alignment starts to precess around $\mathbf{B}_0$, giving rise to a new nonzero component of the alignment $\langle J_xJ_y+J_yJ_x\rangle$. It is the interaction of this alignment with $\mathbf{E}_0$ that gives rise to the orientation $\langle J_z\rangle$ along Oz. In a certain sense, there is an analogy between the motion-induced atomic orientation studied here and the effects described in Refs. 24 and 25 and dealing with the orientation produced by the interaction of an atomic alignment with a real or fictitious electric field.

(ii) One can easily understand why the new cooling mechanism studied in this section does not work for a ground state $J_g = 1/2$. In a $J = 1/2$ state no alignment can exist (Wigner–Eckart theorem). Optical pumping with a linearly polarized light cannot therefore introduce any anisotropy in a $J_g = 1/2$ ground state, at least when v, i.e., $|\mathbf{B}_0|$, is very small. It is only when $|\mathbf{B}_0|$ is large enough to produce Zeeman detuning comparable with Γ that the two counterpropagating laser beams begin to be scattered with different efficiencies, leading to usual Doppler cooling. Another way of interpreting this result is to note that the two sublevels $|g_{\pm 1/2}\rangle_z$ cannot be connected to the same excited state by the two laser polarizations σ^+ and σ^-, so that no coherence can build up between these two sublevels.

5. *Getting Unbalanced Radiation Pressures with a Motion-Induced Atomic Orientation*

Looking at Figs. 1(a) and 5, one sees there is a six times greater probability that an atom in $|g_{-1}\rangle_z$ will absorb a σ^- photon propagating toward $z < 0$ than that it will absorb a σ^+ photon propagating toward $z > 0$. The reverse conclusions can be drawn for an atom in $|g_1\rangle_z$.

If the atom moves toward $z > 0$ and if the detuning δ is negative, we saw above in expression (3.21) that the sublevel $|g_{-1}\rangle_z$ is more populated than $|g_{+1}\rangle_z$. It follows that the radiation pressures exerted by the two σ^- and σ^+ waves will be unbalanced. The atom will scatter more counterpropagating σ^- photons than copropagating σ^+ ones, and its velocity will be damped. Note that here we ignore the Zeeman coherence between $|g_{-1}\rangle_z$ and $|g_{+1}\rangle_z$. We will see in Section 5 that the contribution of such a Zeeman coherence does not change the previous conclusion.

We must emphasize here that the fact that the two radiation pressures become unbalanced when the atom moves is due not to the Doppler effect, as in Doppler cooling, but to a difference of populations in the ground state that is induced by the inertial term [Eq. (3.13)]. It appears clearly in Eq. (3.20) that the dimensionless parameter characterizing this new cooling mechanism is $kv/|\Delta'|$. At low laser power $|\Delta'| \ll \Gamma$, $kv/|\Delta'|$ is much larger than the corresponding parameter kv/Γ characterizing Doppler cooling. Consequently, the new cooling mechanism works at velocities much lower than for Doppler cooling.

We can now give the order of magnitude of the new friction force. The difference between the number of σ^+ and σ^- photons scattered per unit time is, according to Eq. (3.20) and neglecting numerical factors, of the order of

$$(\Pi_{+1} - \Pi_{-1})\Gamma' \sim kv\frac{\Gamma'}{\Delta'}, \tag{3.22}$$

where Γ' is of the order of the mean scattering rate of photons by an atom in the ground state. Since each σ^+ (σ^-) scattered photon transfers to the atom a mean momentum $+\hbar k$ ($-\hbar k$), we conclude that the mean momentum transferred to the atom per unit time, i.e., the mean force F acting upon the atom, is of the order of

$$F \sim \hbar k^2 \frac{\Gamma'}{\Delta'} v. \tag{3.23}$$

F is proportional to v and opposite v since the light shift Δ' is negative for $\delta < 0$; therefore F is a friction force. As in Subsection 3.A we find that F is independent of the laser power at low power since Γ' and Δ' are both proportional to the laser power. Note, however, that the friction coefficient associated with expression (3.23),

$$\alpha \sim -\hbar k^2 \frac{\Gamma'}{\Delta'}, \tag{3.24}$$

is much smaller than expression (3.7), since it varies as Γ'/Δ' instead of Δ'/Γ' and since we suppose here that $\Gamma' \ll |\Delta'|$ [see expression (3.14a)]. We will see, however, in Sections 4 and 5 that the diffusion coefficient associated with expression (3.24) is smaller than the one associated with expression (3.7), so that both configurations lead to equilibrium temperatures of the same order.

6. *Mechanism of Energy Dissipation*

The physical picture presented in the previous subsection clearly shows how the atomic momentum decreases in this new cooling scheme. This is due not, as in the Sisyphus effect of Subsection 3.A.2, to a coherent redistribution of photons between the two counterpropagating waves but to the fact that the atom scatters more photons from one wave than from the other. The two radiation pressures get unbalanced when the atom moves.

We can now try to understand how the atomic kinetic energy is dissipated. In order to have a precise energy balance, we must work in the energy basis $\{|g_m\rangle_y\}$ introduced in Subsection 3.B.3, and we have to wait long enough that we

can reach a steady state and get an energy resolution better than $\hbar|\Delta'|$ for the scattered photons. (Of course, this time should not be too long so that we can neglect any velocity change resulting from the friction force.) It is then clear that the steady-state populations of $\overline{|g_0\rangle_y}$ and $\overline{|g_{\pm1}\rangle_y}$ adjust themselves to values such that the rate of Stokes processes from $\overline{|g_0\rangle_y}$ to $\overline{|g_{+1}\rangle_y}$ balances the rate of anti-Stokes processes from $\overline{|g_{+1}\rangle_y}$ to $\overline{|g_0\rangle_y}$. As in Subsection 3.B.1, we find a fluorescence spectrum that remains symmetric even when the atom moves, since there are always as many Raman Stokes as Raman anti-Stokes photons emitted per unit time. Consequently, it does not seem appropriate, as was done in the first explanations of this cooling mechanism, to invoke direct nonadiabatic transitions between $\overline{|g_0\rangle_y}$ and $\overline{|g_{\pm1}\rangle_y}$ converting kinetic energy into potential energy, this potential energy then being dissipated by Raman anti-Stokes processes.

Actually, for this second cooling scheme the dissipation is, as in Doppler cooling, due to the fact that in the laboratory frame the fluorescence photons have on average a blue Doppler shift on the Rayleigh line as well as on the two Raman lines. Consider, for example, the fluorescence photon following the absorption of a σ^- photon. If it is reemitted toward $z < 0$, it has no Doppler shift in the laboratory frame, whereas it has a Doppler shift $2kv$ when it is reemitted toward $z > 0$. On average, the Doppler energy dissipated by a fluorescence cycle involving a σ^- photon is $\hbar kv$. For a σ^+ photon a similar argument gives $-\hbar kv$. The total Doppler energy dissipated per unit time is therefore equal to

$$\frac{dW}{dt} \sim -\Gamma'(\Pi_{+1} - \Pi_{-1})\hbar kv \sim -\frac{\Gamma'}{\Delta'}\hbar k^2 v^2, \tag{3.25}$$

which coincides with the power $-Fv$ dissipated by the friction force [expression (3.23)].

4. THEORY OF LASER COOLING IN THE lin ⊥ lin CONFIGURATION

This section is devoted to a quantitative study of the cooling mechanism presented in Subsection 3.A. Let us recall that this mechanism is based on a Sisyphus effect induced by a spatial modulation of the light shifts of the atomic Zeeman ground sublevels. As in Subsection 3.A, we study here a $J_g = 1/2 \leftrightarrow J_e = 3/2$ atomic transition and use a semiclassical approach to evaluate the friction force and the equilibrium temperature reached by the atom.

Our treatment is limited to the low-power domain ($\Omega \ll \Gamma$). As explained in the Introduction, this ensures that pumping times τ_p much longer than the radiative lifetime τ_R can appear, which in turn may lead to temperatures well below $\hbar\Gamma$. This low-power hypothesis leads, in addition, to much simpler calculations since it permits a perturbative treatment of the problem.

We also restrict our calculation of the radiative force to the low-velocity domain (Doppler shift $kv \ll \Gamma$). This also introduces an important simplification. Indeed, in this low-velocity domain, optical coherences (density-matrix elements between ground and excited states) and excited-state populations are almost unaffected by atomic motion: The effect of the Doppler shift kv during the relaxation time τ_R (or $2\tau_R$) of these quantities is negligible. Let us, however, emphasize that we do not impose any condition on kv and the inverse Γ' of the pumping time τ_p. Atomic motion can therefore greatly affect the atomic ground-state dynamics and then induce a large velocity-dependent force.

First, we study the internal atomic evolution. Starting from the optical Bloch equations that describe the evolution of the atomic density operator,[26] we obtain two equations giving the evolution of the ground-state populations. We then calculate the average radiative force as a function of the atomic velocity, which gives the friction coefficient and the velocity capture range for this cooling mechanism. Finally, we evaluate the momentum diffusion coefficient and derive the equilibrium temperature of atoms cooled in the lin ⊥ lin configuration.

A. Internal Atomic Evolution

All the calculations of this paper are done in the electric-dipole and rotating-wave approximations so that the atom–laser field coupling can be written as

$$V = -[\mathbf{D}^+ \cdot \mathcal{E}^+(\mathbf{r})\exp(-i\omega_L t) + \mathbf{D}^- \cdot \mathcal{E}^-(\mathbf{r})\exp(i\omega_L t)]. \tag{4.1}$$

$\mathbf{D}^+$ and $\mathbf{D}^-$ are the raising and lowering parts of the atomic electric-dipole operator, and $\mathcal{E}^+$ and $\mathcal{E}^- = (\mathcal{E}^+)^*$ are the positive- and negative-frequency components of the laser electric field. The laser field for the lin ⊥ lin configuration was given in Eq. (2.7). Inserting its value into the atom–field coupling and using the Clebsh–Gordan coefficients indicated in Fig. 2, we get

$$\begin{aligned} V = {} & \frac{\hbar\Omega}{\sqrt{2}} \sin kz \left[|e_{3/2}\rangle\langle g_{1/2}| + \frac{1}{\sqrt{3}} |e_{1/2}\rangle\langle g_{-1/2}| \right] \\ & \times \exp(-i\omega_L t) + \frac{\hbar\Omega}{\sqrt{2}} \cos kz \left[|e_{-3/2}\rangle\langle g_{-1/2}| \right. \\ & \left. + \frac{1}{\sqrt{3}} |e_{-1/2}\rangle\langle g_{1/2}| \right] \exp(-i\omega_L t) + \text{h.c.} \end{aligned} \tag{4.2}$$

Note that, in order to simplify the mathematical expression of V, we shifted the origin on the z axis by an amount $\lambda/8$.[27] In Eq. (4.2), Ω represents the Rabi frequency for each of the two running waves calculated for an atomic transition with a Clebsh–Gordan coefficient equal to 1 and with a reduced dipole moment for the transition equal to d:

$$\Omega = -2\frac{d\mathcal{E}_0}{\hbar}. \tag{4.3}$$

Expression (4.2) also can be interpreted as describing the interaction of the atom with two standing waves, σ^+ and σ^- polarized, and shifted with respect to each other by $\lambda/4$.

The average force acting on the atom can now be derived from the spatial gradient of V:

$$\begin{aligned} f &= \left\langle -\frac{dV}{dz} \right\rangle \\ &= -\frac{\hbar k\Omega}{\sqrt{2}} \cos kz \left[\tilde{\rho}(g_{1/2}, e_{3/2} + \frac{1}{\sqrt{3}} \tilde{\rho}(g_{-1/2}, e_{1/2}) + \text{c.c.} \right] \\ &\quad + \frac{\hbar k\Omega}{\sqrt{2}} \sin kz \left[\tilde{\rho}(g_{-1/2}, e_{-3/2}) + \frac{1}{\sqrt{3}} \tilde{\rho}(g_{1/2}, e_{-1/2}) + \text{c.c.}, \right. \end{aligned} \tag{4.4}$$

with

$$\tilde{\rho}(g_i, e_j) = \langle g_i|\rho|e_j\rangle \exp(-i\omega_L t), \tag{4.5}$$

where ρ is the steady-state density operator.

We now need to calculate the steady-state value of the optical coherences $\tilde{\rho}(g_i, e_j)$, using optical Bloch equations. For example, we have for $\tilde{\rho}(g_{1/2}, e_{3/2})$

$$\dot{\tilde{\rho}}(g_{1/2}, e_{3/2}) = -\left(i\delta + \frac{\Gamma}{2}\right)\tilde{\rho}(g_{1/2}, e_{3/2}) - i\frac{\Omega}{\sqrt{6}}\cos kz\langle e_{-1/2}|\rho|e_{3/2}\rangle + \frac{i\Omega}{\sqrt{2}}\sin kz[\langle g_{1/2}|\rho|g_{1/2}\rangle - \langle e_{3/2}|\rho|e_{3/2}\rangle]. \tag{4.6}$$

This equation is valid for any power and for any atomic velocity $\dot{z}(t)$. It can be simplified in the low-power and low-velocity domains in the following ways:

(i) The low-intensity hypothesis ($\Omega \ll \Gamma$) implies that the populations and coherences of the excited state remain very small compared with the populations of the ground state. Consequently, we can neglect $\langle e_i|\rho|e_j\rangle$ in Eq. (4.6) and calculate $\tilde{\rho}(g_{1/2}, e_{3/2})$ to first order in Ω.

(ii) Since the velocity is low ($kv \ll \Gamma$), the relaxation time $2\Gamma^{-1}$ of optical coherences is much shorter than the typical evolution time of $\sin(kz)$ (of the order of $1/kv$) or of the ground-state populations (τ_p). This means that the optical coherence $\tilde{\rho}(g_{1/2}, e_{3/2})$ follows adiabatically the ground-state population so that we can write

$$\tilde{\rho}(g_{1/2}, e_{3/2}) = \frac{\Omega/\sqrt{2}}{\delta - i\frac{\Gamma}{2}}\Pi_{1/2}\sin kz, \tag{4.7}$$

with

$$\Pi_{\pm 1/2} = \langle g_{\pm 1/2}|\rho|g_{\pm 1/2}\rangle. \tag{4.8}$$

Consequently, we now need to calculate the ground-state populations $\Pi_{\pm 1/2}$ in order to evaluate the force [Eq. (4.4)]. Note that the coherence between the two ground states $\langle g_{1/2}|\rho|g_{-1/2}\rangle$ does not contribute to the calculation and actually has a zero steady-state value for this laser configuration, since it is not coupled to the ground-state populations. This would no longer be true for a more complicated atomic transition for which nonzero steady-state coherences can appear among ground-state sublevels.

In order to calculate $\Pi_{\pm 1/2}$, we now write the optical Bloch equations for excited-state populations; for example, for $\langle e_{3/2}|\rho|e_{3/2}\rangle$:

$$\langle e_{3/2}|\dot{\rho}|e_{3/2}\rangle = -\Gamma\langle e_{3/2}|\rho|e_{3/2}\rangle + i\frac{\Omega}{\sqrt{2}}\sin kz[\tilde{\rho}(e_{3/2}, g_{1/2}) - \tilde{\rho}(g_{1/2}, e_{3/2})]. \tag{4.9}$$

In this equation we replace the optical coherences by their expressions in terms of ground-state populations. Now, since the relaxation time of the excited-state populations is Γ^{-1}, we can again note that they follow adiabatically the variations of the ground-state populations so that

$$\langle e_{3/2}|\rho|e_{3/2}\rangle = s_0\,\Pi_{1/2}\sin^2 kz, \tag{4.10}$$

where s_0 is the detuning-dependent saturation parameter

$$s_0 = \frac{\Omega^2/2}{\delta^2 + \frac{\Gamma^2}{4}}. \tag{4.11}$$

Finally, we write the optical Bloch equations for the ground-state populations. For example, we have for $\Pi_{1/2}$

$$\dot{\Pi}_{1/2} = \Gamma\left[\langle e_{3/2}|\rho|e_{3/2}\rangle + \frac{2}{3}\langle e_{1/2}|\rho|e_{1/2}\rangle + \frac{1}{3}\langle e_{-1/2}|\rho|e_{-1/2}\rangle\right] + \left[\frac{i\Omega}{\sqrt{2}}\tilde{\rho}(g_{1/2}, e_{3/2})\sin kz + \frac{i\Omega}{\sqrt{6}}\tilde{\rho}(g_{1/2}, e_{-1/2})\cos kz + \text{c.c.}\right]. \tag{4.12}$$

We insert the expressions of optical coherences and excited-state populations in terms of $\Pi_{\pm 1/2}$ to get

$$\dot{\Pi}_i = -\frac{1}{\tau_p}[\Pi_i - \Pi_i^{\text{st}}(z)], \tag{4.13}$$

where the pumping time τ_p and the stationary populations $\Pi_i^{\text{st}}(z)$ are given by

$$1/\tau_p = \Gamma' = 2\Gamma s_0/9, \tag{4.14a}$$

$$\Pi_{1/2}{}^{\text{st}}(z) = \sin^2 kz, \qquad \Pi_{-1/2}{}^{\text{st}}(z) = \cos^2 kz. \tag{4.14b}$$

For an atom at rest in z the populations $\Pi_i(z)$ reach their stationary value in a time τ_p inversely proportional to the laser power, as mentioned in the Introduction. We also note that these stationary populations are strongly modulated in space (see Fig. 3).

B. Force in the lin ⊥ lin Configuration

In order to calculate the radiative force f [Eq. (4.4)], we first replace the optical coherences contributing to f by their expressions in terms of the ground-state populations. This leads to

$$f = -\frac{2}{3}\hbar k\delta s_0\,(\Pi_{1/2} - \Pi_{-1/2})\sin 2kz. \tag{4.15}$$

This expression has a clear physical meaning in terms of light shifts: The two levels $g_{1/2}$ and $g_{-1/2}$ are light-shifted by a quantity that corresponds to the sum of the two light shifts created by the two σ^+ and σ^- standing waves appearing in expression (4.2) of the laser–atom coupling V. We can indeed add these two terms independently in the low-intensity domain since the two states $g_{1/2}$ and $g_{-1/2}$ are not connected to the same excited sublevel. Using the Clebsh–Gordan coefficients given in Fig. 2, we obtain

$$\Delta E_{1/2} = \hbar\Delta_+{}' = \hbar\delta s_0\left(\sin^2 kz + \frac{1}{3}\cos^2 kz\right) = E_0 - \frac{\hbar\delta s_0}{3}\cos 2kz,$$

$$\Delta E_{-1/2} = \hbar\Delta_-{}' = \hbar\delta s_0\left(\cos^2 kz + \frac{1}{3}\sin^2 kz\right) = E_0 + \frac{\hbar\delta s_0}{3}\cos 2kz, \tag{4.16}$$

where

$$E_0 = \frac{2}{3}\hbar\delta s_0. \tag{4.17}$$

As sketched in Fig. 3, the two light-shifted ground-state sublevels oscillate in space with a period $\lambda/2$. This spatial dependence then causes a state-dependent force; taking the gradient of $\Delta E_{\pm 1/2}$, we get

$$f_{\pm 1/2} = -\frac{d}{dz}\Delta E_{\pm 1/2} = \mp\frac{2}{3}\hbar k\delta s_0 \sin 2kz, \tag{4.18}$$

so that the average force [Eq. (4.15)] can be written as

$$f = f_{1/2}\Pi_{1/2} + f_{-1/2}\Pi_{-1/2}. \tag{4.19}$$

This force f is then just the average of the two state-dependent forces $f_{\pm 1/2}$ weighted by the populations of these states. Such an expression is similar to the one obtained for a two-level atom in intense laser light, provided that the levels $g_{\pm 1/2}$ are replaced by the two dressed levels.[16] However, an important difference arises here since each of the two levels involved in Eq. (4.19) is essentially a ground-state sublevel with a long residence time τ_p. By contrast, in the two-level problem the two dressed states were strongly contaminated by the excited state, so that their lifetime was $\simeq\Gamma^{-1}$.

We now calculate the populations $\Pi_{\pm 1/2}$ in order to evaluate the force from Eq. (4.19). First, we take an atom at rest. These two populations are then equal to their steady-state value [Eq. (4.14b)], so that we obtain

$$f(z, v = 0) = \frac{2}{3}\hbar k\delta s_0 \sin 2kz \cos 2kz = -\frac{dU}{dz}, \tag{4.20}$$

where the potential U is given by

$$U(z) = -\frac{1}{6}\hbar\delta s_0 \sin^2 2kz. \tag{4.21}$$

The fact that $f(z, v = 0)$ derives from a potential is again similar to the corresponding result for the dipole force acting on a two-level atom in a standing wave.

We now consider a very slow atom for which the Doppler shift kv is smaller than $1/\tau_p$. Note that this condition is much more stringent than the condition $kv \ll \Gamma$ required for writing Eq. (4.7) or (4.10). For such very slow atoms, the effect of atomic motion on the populations $\Pi_{\pm 1/2}$ can be treated pertubatively by an expansion in terms of the small parameter $kv\tau_p$:

$$\Pi_i(z, v) = \Pi_i^{st}(z) - v\tau_p\frac{d\Pi_i^{st}}{dz} + \cdots \tag{4.22}$$

We insert these expressions into the result [Eq. (4.19)] for the force, and we get

$$f(z, v) = f(z, v = 0) - v\tau_p\sum_{i=\pm 1/2} f_i\frac{d\Pi_i^{st}}{dz} = f(z, v = 0) + \frac{4}{3}\hbar k^2\delta s_0 v\tau_p \sin^2(2kz). \tag{4.23}$$

We now average this result over a wavelength. The average of $f(z, v = 0)$ is zero, so that we get

$$\bar{f}(v) = -\alpha v, \tag{4.24}$$

where the friction coefficient α is equal to

$$\alpha = -\frac{2}{3}\hbar k^2\delta s_0\tau_p \qquad (\delta < 0) \tag{4.25}$$

or, using Eq. (4.14a),

$$\alpha = -3\hbar k^2\frac{\delta}{\Gamma} \qquad (\delta < 0). \tag{4.26}$$

We therefore get a friction coefficient independent of the laser power [see relation (3.9)]. On the other hand, the range of validity of the result [Eq. (4.24)] is proportional to laser power. Indeed, the expansion (4.22) requires $kv \ll 1/\tau_p$, where $1/\tau_p$ is proportional to laser power.

Finally, we come to the calculation of the force on the whole range $kv \ll \Gamma$ with no restriction on the relative values of kv and $1/\tau_p$. The evolution equations (4.13) are still valid, but they can no longer be solved by a perturbative expansion such as Eq. (4.22). Fortunately, it is possible to get an exact solution for the forced regime of Eq. (4.13):

$$\Pi_{\pm 1/2}(z, v) = \frac{1}{2}\left(1 \mp \frac{\cos 2kz + 2kv\tau_p \sin 2kz}{1 + 4v^2{\tau_p}^2}\right). \tag{4.27}$$

Inserting this result into expression (4.19) for the force and averaging over a wavelength, we obtain

$$\bar{f}(v) = \frac{-\alpha v}{1 + (v^2/v_c^2)}, \tag{4.28}$$

where the critical velocity v_c is

$$kv_c = 1/2\tau_p. \tag{4.29}$$

As predicted in Subsection 3.A.3, the force is maximal in this configuration when $v = v_c$, that is, when the distance covered during a pumping time is of the order of the spatial period of the modulated light shifts. In Fig. 7 we have plotted this force versus v (solid curve). Note that expression (4.28) of the force is valid only for $kv \ll \Gamma$. Outside this range, the polarization gradient cooling becomes inefficient, and the dominant process is Doppler cooling. For this lin ⊥ lin configuration, we did not calculate the full velocity dependence of the force, which would allow one to study the transition between the two cooling regimes. In Fig. 7 we plotted just (dotted curve) the force that one would get by independently summing the two radiation pressure forces exerted by each Doppler-shifted wave. The differences between the slopes at $v = 0$ (friction coefficients) and between the capture ranges appear clearly.

To sum up, we obtained an analytical expression for the velocity-dependent force [Eq. (4.28)] that gives both the friction coefficient α (slope at origin) and the velocity capture range v_c.

C. Equilibrium Temperature in the lin ⊥ lin Configuration

We now turn to the problem of evaluating the equilibrium temperature in this new cooling scheme. We first evaluate the momentum diffusion coefficient D_p and then calculate the equilibrium temperature resulting from the competition between the cooling described above and the heating from diffusion

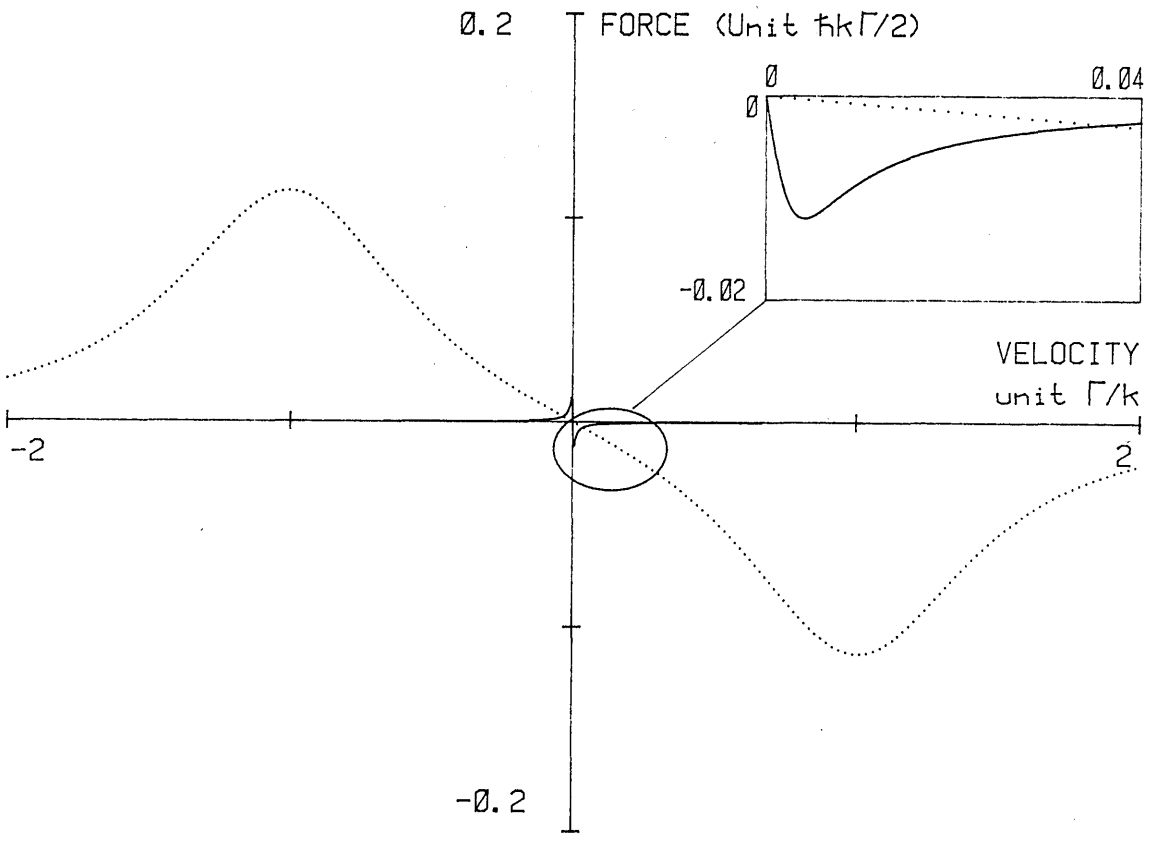

Fig. 7. Variations with velocity v of the force due to polarization gradients in the lin ⊥ lin configuration for a $J_g = 1/2 \leftrightarrow J_e = 3/2$ transition (solid curve). The values of the parameters are $\Omega = 0.3\Gamma$, $\delta = -\Gamma$. The dotted curve shows sum of the two radiation pressure forces exerted independently by the two Doppler-shifted counterpropagating waves. The force due to polarization gradients leads to a much higher friction coefficient (slope at $v = 0$) but acts on a much narrower velocity range.

$$k_B T = \frac{D_p}{\alpha}. \tag{4.30}$$

Finally, we discuss the validity of the semiclassical approximation used throughout this calculation.

In order to calculate the exact value of D_p, one could compute the correlation function of the force operator.[12,13] For a multilevel atom, such a calculation would be rather tedious, so that we prefer to use a heuristic calculation here.

There are three main contributions to D_p; the two first ones are already present for a $J_g = 0 \leftrightarrow J_e = 1$ transition,[21] and the third one is specific of an atom with several ground-state sublevels:

(i) There are fluctuations of the momentum carried away by fluorescence photons.

(ii) There are fluctuations in the difference among the number of photons absorbed in each of the two laser waves.

(iii) There are fluctuations of the instantaneous dipole force oscillating back and forth between $f_{1/2}(z)$ and $f_{-1/2}(z)$ at a rate $1/\tau_p$.

For a $J_g = 0 \leftrightarrow J_e = 1$ transition,[21] the two first contributions give for a dipole radiation pattern

$$\overline{D_p'} = \frac{7}{10}\hbar^2 k^2 \Gamma s_0. \tag{4.31}$$

We assume that Eq. (4.31) still gives the good order of magnitude for these two contributions in the case of a $J_g = 1/2 \leftrightarrow J_e = 3/2$ transition. To evaluate the third contribution (coefficient D_p''), we start from

$$D_p'' = \int_0^\infty d\tau [\overline{f(t)f(t+\tau)} - \bar{f}^2], \tag{4.32}$$

which must be calculated for an atom at rest in z (the label z was omitted for simplification). The force $f(t)$ oscillates between $f_{1/2}(z)$ and $f_{-1/2}(z)$, and its correlation function can be written as

$$\overline{f(t)f(t+\tau)} = \sum_{i=\pm 1/2} \sum_{j=\pm 1/2} f_i f_j P(i, t; j, t+\tau), \tag{4.33}$$

where $P(i, t; j, t+\tau)$ represents the probability of being in state i at time t and in state j at time $t+\tau$. The calculation is then similar to the one done to evaluate the fluctuations of the dipole force for a two-level atom (Ref. 16, Subsection 4B), and it leads to

$$D_p'' = 4[f_{1/2}(z)]^2 \Pi_{1/2}^{st}(z) \Pi_{-1/2}^{st}(z) \tau_p$$

$$= 2\hbar^2 k^2 \frac{\delta^2}{\Gamma} s_0 \sin^4(2kz). \tag{4.34}$$

Once this is averaged over a wavelength, it gives

$$\overline{D_p''} = \frac{3}{4}\hbar^2 k^2 \frac{\delta^2}{\Gamma} s_0. \tag{4.35}$$

This second coefficient exceeds the first one as soon as $|\delta|$ is larger than Γ. Therefore, neglecting $\bar{D}_p'$, we get

$$|\delta| \gg \Gamma \Rightarrow k_B T = \frac{D_p}{\alpha} \simeq \frac{\hbar|\delta|}{4} s_0 \tag{4.36}$$

or, using definition (4.11) for s_0,

$$|\delta| \gg \Gamma \Rightarrow k_B T \simeq \frac{\hbar\Omega^2}{8|\delta|}. \tag{4.37}$$

It appears in these expressions that the residual kinetic energy is of the order of the light shift $\hbar\Delta'$ of the ground state. This simple result must be compared with the one obtained for a two-level system [Eq. (1.2)]. It may lead to a much lower temperature, and it is consistent with two experimental observations,[7-9] as long as the other hyperfine levels of the transition can be ignored:

(i) At a given power (Ω fixed), the temperature decreases when the detuning increases.
(ii) At a given detuning, reducing the power decreases the temperature.

Another important remark concerns the comparison between the residual kinetic energy $k_B T/2$ and the potential $U(z)$ derived in Eq. (4.21). We actually find that these two quantities are of the same order, which indicates that in the stationary state atoms are bunched around the points $z = n\lambda/4$ rather than uniformly distributed. In this regime, one should then correct expression (4.24) for the force, which was obtained by assuming a constant velocity. A Monte Carlo simulation, similar to the one in Ref. 28, is probably the best way to derive precise results concerning the stationary state in this configuration.

Finally, let us look for the lowest temperatures achievable in this configuration. Expression (4.37) suggests that an arbitrarily low temperature could be reached, for instance, by decreasing the laser power. Actually, this is not true. Indeed one must check that the rms velocity deduced from expression (4.37) is well below the critical velocity v_c [Eq. (4.29)], so that the cooling force is indeed linear for all velocity classes contributing to the stationary state. We therefore get

$$v_{\text{rms}} \ll v_c \Rightarrow \Omega \gg \sqrt{\frac{\hbar k^2}{M}\frac{|\delta|^3}{\Gamma^2}}, \tag{4.38}$$

which puts a lower bound on the laser power required for our treatment to be valid. This in turn gives a lower bound on the achievable rms velocity:

$$v_{\text{rms}} \gg \frac{\hbar k}{M}\frac{|\delta|}{\Gamma}. \tag{4.39}$$

Consequently, the lowest achievable rms velocity in this model remains larger than the recoil velocity. Let us recall that the recoil velocity was, in any event, a limit for the validity of our semiclassical treatment.

We are currently working on a full quantum treatment of cooling in the lin $\perp$ lin configuration, analogous to the one presented at the end of Subsection 5.D for the σ^+–σ^- configuration. Note that such a treatment in the present configuration is more complicated than for the σ^+–σ^- one, owing to the possibility that photons are coherently redistributed between the two waves.

5. THEORY OF LASER COOLING IN THE σ^+–σ^- CONFIGURATION

Now we come to this final section of this paper, which is devoted to the quantitative study of laser cooling in a σ^+–σ^- configuration for a $J_g = 1 \leftrightarrow J_e = 2$ atomic transition.

As shown in Section 2, the polarization gradient is then quite different from the one studied in Section 4: The polarization is linear in any place and rotates along the propagation axis Oz on the length scale λ.

Cooling in this configuration originates from two quite distinct processes. The first is the usual Doppler cooling that results from differential absorption of the σ^+ and σ^- waves when the Doppler shift kv is a nonnegligible part of the natural width Γ. The second mechanism, qualitatively studied in Subsection 3.B, originates from the enhancement of radiation pressure imbalance that is due to a sensitive motion-induced atomic orientation. We study here the case of a $J_g = 1 \leftrightarrow J_e = 2$ transition (Fig. 5), which, as explained in Subsection 3.B, is the simplest atomic transition exhibiting this sensitive velocity-induced orientation. For simplification, we also use at the end of this section a fictitious W atom, which can be formally obtained from the real 1–2 transition by removing the V system formed by $|g_0\rangle$, $|e_{-1}\rangle$, $|e_{+1}\rangle$.

A. Various Velocity Domains

As in Section 4, we restrict our treatment to the low-intensity domain ($\Omega \ll \Gamma$, leading to $\tau_p \gg \tau_r$ or equivalently to $\Gamma' \ll \Gamma$). This also allows for a perturbative treatment of the problem: One needs to consider only the density matrix in the ground state (3×3 elements) instead of the total atomic density matrix (8×8 elements). In this low-intensity regime, we can distinguish three velocity domains:

(i) For very low velocities ($kv \ll \Gamma'$), we expect the force to be linear with velocity. In order to calculate this force, we need to take into account all coherences among the various ground-state sublevels, since the coupling between populations and coherences is responsible for the motion-induced orientation.
(ii) In the intermediate regime ($\Gamma' \ll kv \ll \Gamma$), the precession frequency kv of the coherences among ground-state sublevels [owing to the inertial term in Eq. (3.13)] is large compared with their damping time τ_p, and these coherences cannot build up. Consequently, the new cooling force decreases. On the other hand, the Doppler shift kv is still small compared with Γ, so that the usual Doppler-cooling force remains small.
(iii) For higher velocities ($kv \gtrsim \Gamma$), the coherences among the ground-state sublevels are completely negligible, and the Doppler shift is now comparable to the natural width. In this domain, the force is then practically equal to the usual Doppler cooling force.

B. Calculation of the Cooling Force

In order to calculate the steady-state radiative force, we start with the atom–laser coupling [Eq. (4.1)], which we

write in the atomic reference frame. Using expressions (2.2) and (2.3) for the laser electric field, we get

$$V = \frac{\hbar\Omega}{2}\left[|g_1\rangle\langle e_2| + \frac{1}{\sqrt{2}}|g_0\rangle\langle e_1| + \frac{1}{\sqrt{6}}|g_{-1}\rangle\langle e_0|\right] \times \exp[i(\omega_- t - kz)] + \text{h.c.} + \frac{\hbar\Omega}{2}\left[|g_{-1}\rangle\langle e_{-2}| + \frac{1}{\sqrt{2}}|g_0\rangle\langle e_{-1}| + \frac{1}{\sqrt{6}}|g_1\rangle\langle e_0|\right] \times \exp[i(\omega_+ t - kz)] + \text{h.c.}, \quad (5.1)$$

where we have put

$$\Omega = -2d\mathcal{E}_0/\hbar \quad \text{[identical to Eq. (4.3)]},$$
$$\omega_\pm = \omega_L \pm kv. \quad (5.2)$$

The first (third) line of Eq. (5.1) describes the coupling with the σ^+ (σ^-) laser wave propagating toward $z > 0$ ($z < 0$). As in Section 4, the semiclassical force is obtained from the average value of the gradient of the coupling V. Assuming that the atom is at the point $z = 0$ in its reference frame, we get

$$\mathbf{f} = i\hbar\mathbf{k}\Omega\left[\tilde{\rho}(e_2, g_1) + \frac{1}{\sqrt{2}}\tilde{\rho}(e_1, g_0) + \frac{1}{\sqrt{6}}\tilde{\rho}(e_0, g_{-1})\right] + \text{c.c.} - i\hbar\mathbf{k}\Omega\left[\tilde{\rho}(e_{-2}, g_{-1}) + \frac{1}{\sqrt{2}}\tilde{\rho}(e_{-1}, g_0) + \frac{1}{\sqrt{6}}\tilde{\rho}(e_0, g_1)\right] + \text{c.c.}, \quad (5.3)$$

where the coefficients $\tilde{\rho}$ are defined by

$$\tilde{\rho}(e_{i\pm1}, g_i) = \langle e_{i\pm1}|\rho|g_i\rangle \exp(i\omega_\mp t). \quad (5.4)$$

Actually, these coefficients are nothing but the matrix elements of ρ in the moving rotating frame defined in Subsection 3.C.2.

We now need to evaluate the steady-state value of the optical coherences $\tilde{\rho}(e_i, g_j)$. This is done using optical Bloch equations, which give the evolution of the atomic density operator ρ.[26] Let us, for example, write down the equation for $\tilde{\rho}(e_1, g_0)$:

$$\dot{\tilde{\rho}}(e_1, g_0) = \left[i(\delta - kv) - \frac{\Gamma}{2}\right]\tilde{\rho}(e_1, g_0) + \frac{i\Omega}{2\sqrt{2}}[\langle e_1|\rho|e_1\rangle + \langle e_1|\rho|e_{-1}\rangle \exp(-2ikvt) - \langle g_0|\rho|g_0\rangle]. \quad (5.5)$$

In this equation, $\langle e_1|\rho|e_1\rangle$ and $\langle e_1|\rho|e_{-1}\rangle$ can be neglected compared with $\langle g_0|\rho|g_0\rangle$ because of the low-power hypothesis. We then get in steady state

$$\tilde{\rho}(e_1, g_0) = \frac{\Omega/2\sqrt{2}}{\delta - kv + i\frac{\Gamma}{2}}\Pi_0, \quad (5.6)$$

where

$$\Pi_i = \langle g_i|\rho|g_i\rangle. \quad (5.7)$$

We can, in this way, calculate all optical coherences in terms of the ground-state populations Π_i and coherences among these states. Note that, because of the structure of the laser excitation, the only nonzero Zeeman coherence in steady state is the coherence between g_1 and g_{-1}. We put in the following:

$$C_r = \text{Re}[\langle g_1|\rho|g_{-1}\rangle \exp(-2ikvt)],$$
$$C_i = \text{Im}[\langle g_1|\rho|g_{-1}\rangle \exp(-2ikvt)]. \quad (5.8)$$

Once all optical coherences have been calculated, it is possible to get a new expression for the force [Eq. (5.3)]. The detailed calculation is rather long and tedious and is presented in Appendix B. Here, we give only the main results. First we get for the force

$$\mathbf{f} = \hbar\mathbf{k}\frac{\Gamma}{2}\left[\Pi_1\left(s_+ - \frac{s_-}{6}\right) + \Pi_0\left(\frac{s_+ - s_-}{2}\right) + \Pi_{-1}\left(\frac{s_+}{6} - s_-\right) + C_r\left(\frac{s_+ - s_-}{6}\right) - \frac{1}{3}C_i\left(s_+\frac{\delta - kv}{\Gamma} + s_-\frac{\delta + kv}{\Gamma}\right)\right], \quad (5.9)$$

where

$$s_\pm = \frac{\Omega^2/2}{(\delta \mp kv)^2 + \frac{\Gamma^2}{4}} \ll 1 \quad (5.10)$$

represents the saturation parameter of each of the two waves $\sigma^\pm$ for the strongest corresponding transition ($g_{\pm1} \rightarrow e_{\pm2}$). Each term has a clear meaning in expression (5.9) for the force. Take, for instance, an atom in the state g_1. In a time interval dt, it scatters on the average $\Gamma s_+ dt/2$ photons from the σ^+ wave and $\Gamma s_- dt/12$ photons from the σ^- wave (see the Clebsh–Gordan coefficients of Fig. 5). The resulting radiation pressure force, weighted by the population Π_1 of g_1, is therefore equal to the first term of Eq. (5.9). The second and third terms of Eq. (5.9) describe in the same way the radiation pressure force when the atom is in the states g_0 and g_{-1}. Finally, the last two terms, which involve the laser-induced coherence between g_1 and g_{-1}, describe the force induced by the limited photon redistribution that takes place when the atom jumps between g_1 and g_{-1} by absorption-stimulated emission cycles (see Subsection 2.C).

Now we must calculate the five ground-state variables Π_0, $\Pi_{\pm1}$, C_r, C_i. This is done again by using optical Bloch equations, through elimination of the excited-state populations and coherences. One is then left with a closed system of five equations involving only these five required ground-state variables. This elimination is done in Appendix B of this paper. In the very low-velocity domain ($kv\tau_p \ll 1$) these equations lead to the following solutions, to first order in $kv\tau_p = kv/\Gamma' \simeq kv/s_0\Gamma$:

$$\Pi_{\pm1} = \frac{1}{34}\left(13 \pm 240\frac{kv}{s_0\Gamma}\frac{\delta\Gamma}{5\Gamma^2 + 4\delta^2}\right),$$
$$\Pi_0 = \frac{4}{17},$$
$$C_r = \frac{5}{34},$$
$$C_i = -\frac{60}{17}\frac{kv}{s_0\Gamma}\frac{\Gamma^2}{5\Gamma^2 + 4\delta^2}, \quad (5.11)$$

where we have put, as in Section 4 [cf. Eq. (4.11)],

$$s_0 = \frac{\Omega^2/2}{\delta^2 + (\Gamma^2/4)}. \tag{5.12}$$

We can note that these results are in agreement with the ones obtained in Section 3. First, for an atom at rest, it is easy to show that the nondiagonal density matrix obtained here in the $|g_m\rangle_z$ basis indeed leads to the diagonal density matrix obtained in Subsection 3.B in the $|g_m\rangle_y$ basis. Second, the population difference $\Pi_1 - \Pi_{-1}$ calculated from Eqs. (5.11) is equal to the one predicted in Eq. (3.20) in the limit $|\delta| \gg \Gamma$. (In this limit, one indeed gets for the light shift Δ_0' of $|g_0\rangle_y$ the value $\Delta_0' = \Omega^2/3\delta$.)

We are now able to calculate the force in this low-velocity domain. First we note that Eq. (5.9) can be greatly simplified; by neglecting all terms in kv/Γ and keeping only terms in kv/Γ', we get

$$f = \frac{\hbar k \Gamma}{2} s_0 \left[\frac{5}{6} (\Pi_1 - \Pi_{-1}) - \frac{2}{3} \frac{\delta}{\Gamma} C_i \right]. \tag{5.13}$$

The first term of Eq. (5.13) has already been estimated in Subsection 3.B, whereas the second one describes the effect of limited photon redistribution.

Now by inserting the result [Eqs. (5.11)] for the atomic density matrix into the force, we obtain

$$f = -\alpha v,$$
$$\alpha = \frac{120}{17} \frac{-\delta\Gamma}{5\Gamma^2 + 4\delta^2} \hbar k^2. \tag{5.14}$$

The contribution of the population term $5/6(\Pi_1 - \Pi_{-1})$ represents 4/5 of the total result for the friction coefficient α, the remaining 1/5 part being due to $2\delta C_1/3$.

As expected, we get in this low-velocity domain a force linear with velocity, with a damping coefficient (for negative detunings) independent of power. This damping coefficient is maximal for a detuning $\delta = -\Gamma\sqrt{5/4}$, where the force is of the order of $-0.8\hbar k^2 v$. We find here a result that was already mentioned in Subsection 3.B: For $|\delta| \gg \Gamma$, the friction coefficient in the σ^+–σ^- configuration, which varies as Γ/δ, is much smaller than the friction coefficient for the lin $\perp$ lin configuration, which is proportional to δ/Γ [Eq. (4.26)]. Furthermore, we see here that, even for the optimum detuning, the σ_+–σ_- damping coefficient is four times smaller than the lin $\perp$ lin one.

We now come to the complete calculation of the force for any atomic velocity in the low-power approximation. This is done by keeping all the velocity-dependent terms in expressions like (5.6) and by using Eq. (5.9) for the force instead of the simplified expression (5.13). The result of such a calculation (which is detailed in Appendix B) is represented in Fig. 8. In the low-velocity domain, we again find the friction force just calculated above (see, in particular, the inset of Fig. 8). Outside this domain, the force appears to be close to the usual Doppler force, represented by dotted curves. This Doppler force is calculated by neglecting all coherences among ground-state sublevels, so that ground-state populations are obtained only from rate equations:

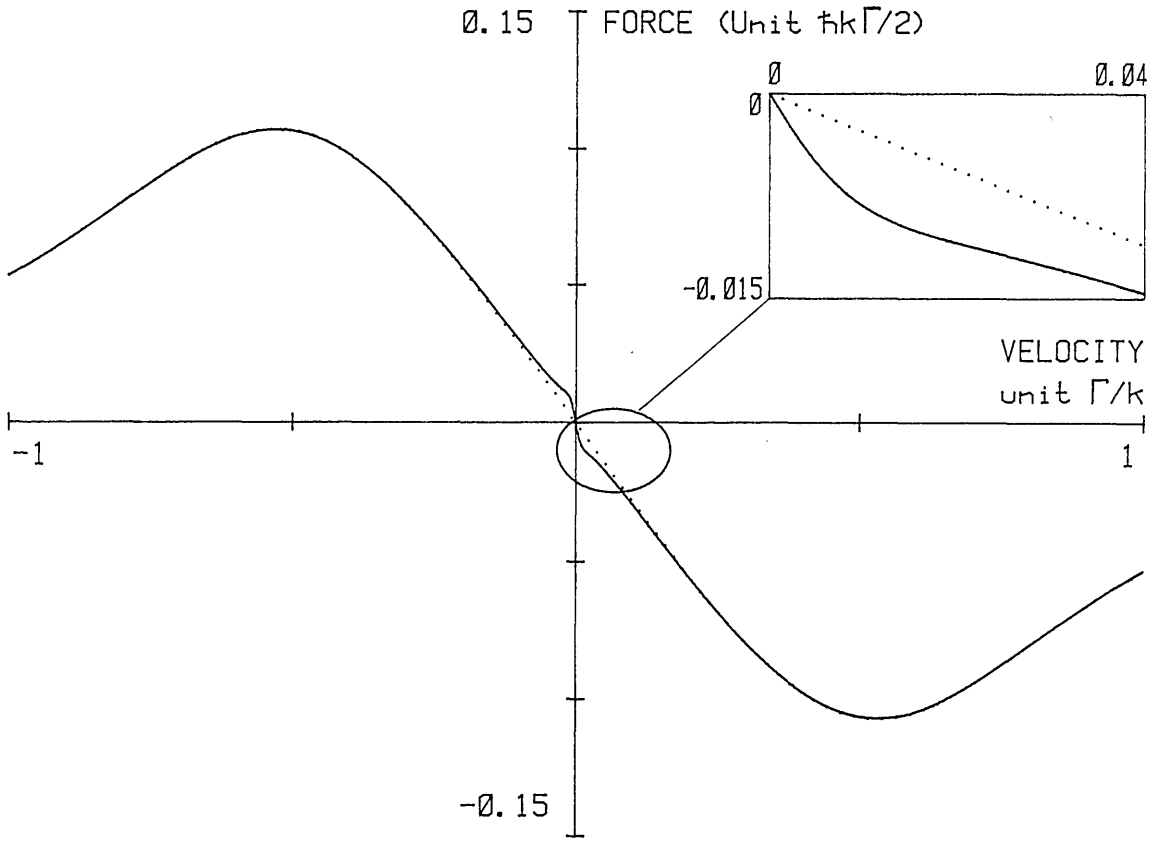

Fig. 8. Variations with velocity of the steady-state radiative force for a $J_g = 1 \leftrightarrow J_e = 2$ transition in the σ_+–σ_- configuration ($\Omega = 0.25\ \Gamma$; $\delta = -0.5\ \Gamma$). The slope of the force near $v = 0$ is very high (see also inset), showing that there is polarization gradient cooling. This new cooling force acts in the velocity range $kv \sim \Delta'$. Outside this range, the force is nearly equal to the Doppler force (shown by the dotted curve) calculated by neglecting all coherences between ground-state sublevels $|g_m\rangle_z$.

$$\Pi_{\pm 1} = \frac{3s_{\pm}(s_{\mp} + 5s_{\pm})}{15(s_+^2 + s_-^2) + 14s_+s_-},$$

$$\Pi_0 = \frac{8s_+s_-}{15(s_+^2 + s_-^2) + 14s_+s_-}. \quad (5.15)$$

We therefore confirm quantitatively that the new cooling force mainly acts in the $kv < \Gamma'$ domain.

C. Equilibrium Temperature in the σ^+-σ^- Configuration

In order to evaluate the equilibrium temperature in this configuration, we first need to evaluate the momentum diffusion coefficient D_p. The exact calculation of D_p is sketched at the end of Appendix B. It uses a method suggested to us by Castin and Molmer[29] and leads to

$$D_p = D_1 + D_2, \quad (5.16)$$

$$D_1 = \frac{18}{170}\hbar^2k^2\Gamma s_0,$$

$$D_2 = \left[\frac{36}{17}\frac{1}{1 + (4\delta^2/5\Gamma^2)} + \frac{4}{17}\right]\hbar^2k^2\Gamma s_0. \quad (5.17)$$

Such an expression can be understood by simple momentum-conservation arguments. Since there are no dipole forces in the σ^+-σ^- configuration, the momentum diffusion is due only to the first two mechanisms mentioned at the beginning of Subsection 4.C.

The first term of Eq. (5.16) (D_1) corresponds to the fluctuations of the momentum carried away by fluorescence photons. The second term (D_2) corresponds to the fluctuations of the difference between the number of photons absorbed in each wave. For large detunings ($|\delta| \gg \Gamma$), D_1 and D_2 are of the same order, as for a $J_g = 0 \leftrightarrow J_e = 1$ transition.[21] By contrast, for small δ, D_2 becomes much larger than D_1. As pointed out to us by Molmer and Castin,[29] this enhancement of D_2 is a consequence of correlations introduced by optical pumping between the directions of two successively absorbed photons. Immediately after a cycle involving the absorption of a σ^+ photon, the atom is more likely to be in the $|g_1\rangle_z$ state and is therefore more likely to absorb another σ^+ photon rather than a σ^- one. As a consequence, the steps of the random walk in momentum space (due to absorption) can be several $\hbar k$ instead of $\hbar k$, and this can increase D_2 for a given saturation parameter by a factor as large as 10. Of course, such an argument holds only if the atom remains in $|g_1\rangle_z$ for a time $\tau_p = 1/\Gamma'$, which is the mean time between two successive fluorescence cycles. If this is not the case, i.e., if the populations are redistributed among the three Zeeman sublevels in g in a time shorter than τ_p, the previous memory effect and, consequently, the large-step random walk, disappear, leading to a small value of D_2 and thus to low temperatures. At low velocities ($kv \ll |\Delta'|$), such a fast redistribution of populations in g occurs at large detuning, as we show now. Since the true stationary states of the systems are the $\{|g_m\rangle_y\}$ states, separated by a splitting of the order of $\hbar\Delta'$, Rabi oscillations between $|g_{+1}\rangle_z$ and $|g_{-1}\rangle_z$ occur at the frequency $|\Delta'|$. If $|\Delta'| \ll \Gamma'$, i.e., if $|\delta| \ll \Gamma$, $|g_{+1}\rangle_z$ can be considered nearly stationary on a time scale τ_p. By contrast, if $|\Delta'| \gg \Gamma'$, i.e., if $|\delta| \gg \Gamma$, the Rabi oscillations in g are fast enough to redistribute completely the populations in g in a time τ_p. This explains why the enhancement of D_2 disappears at large δ [see Eqs. (5.17)].

The result [Eq. (5.16)] can now be used to get the equilibrium temperature

$$k_BT = \frac{\hbar\Omega^2}{|\delta|}\left[\frac{29}{300} + \frac{254}{75}\frac{\Gamma^2/4}{\delta^2 + (\Gamma^2/4)}\right]. \quad (5.18)$$

For large $|\delta|$, this result is quite similar to the one obtained in the lin $\perp$ lin configuration [expression (4.37)]. In particular, it is proportional to laser power and decreases as $1/\delta$ when $|\delta|$ increases. Note that for intermediate detunings ($\Gamma/2 \leqslant |\delta| \leqslant 3\Gamma$), D_2 remains larger than D_1, so that k_BT varies approximately as $1/\delta^3$.

The validity of the result [Eq. (5.18)] is obtained as in Section 4. The only change concerns the condition that the velocities must satisfy in order to get a linear force. Such a condition is now $kv \ll |\Delta'|$ (see Section 3). An argument analogous to the one given at the end of Section 4 then leads to (for $|\delta| \gtrsim \Gamma$)

$$k\bar{v} \ll |\Delta'| \Rightarrow \Omega \gg \sqrt{\frac{\hbar k^2}{M}\delta} \Rightarrow \bar{v} \gg \frac{\hbar k}{M}. \quad (5.19)$$

This limit is smaller than the one found in the lin $\perp$ lin case [expression (4.39)] when the detuning δ is large compared with Γ

D. Principle of a Full Quantum Treatment

It is clear from the result obtained above that, for sufficiently low power, the cooling limit becomes of the order of the one-photon recoil energy. As emphasized in the Introduction, a semiclassical treatment then is no longer possible.

We present here the principle of a treatment in which atomic motion is treated in a full quantum way. For simplicity, we considered a W transition, sketched in Fig. 9(a), instead of the real $J = 1 \leftrightarrow J = 2$ transition. We use the concept of closed families of states introduced in Refs. 18 and 19: In the σ^+-σ^- configuration, the set of states

$$\mathcal{F}(p) = \{|e_{-2}, p - 2\hbar k\rangle, |g_{-1}, p - \hbar k\rangle, |e_0, p\rangle, |g_1, p + \hbar k\rangle, |e_2, p + 2\hbar k\rangle\}$$

is closed with respect to absorption and stimulated-emission processes, and transfers between families occur only via spontaneous-emission processes. Then it is possible to show that the total atomic density operator in steady state has nonzero matrix elements only among states belonging to the same family. This greatly simplifies the study of the evolution of this density matrix: If one wants to take, for instance, 1000 points in momentum space, one has to consider only a $N_\rho \times 1000$ vector instead of a $N_\rho \times [1000]^2$ square matrix; N_ρ is the size $[(2J_g + 1) + (2J_e + 1)]^2$ of the internal atomic density matrix.

Using the generalized optical Bloch equations including recoil,[18,19] we studied the evolution of the atomic momentum distribution for a W atom with a linewidth $\hbar\Gamma$ equal to 400 times the recoil energy $\hbar^2k^2/2M$ (analogous to sodium). A typical result is presented in Fig. 9(b). The initial distribution is Gaussian with a rms width of $16\hbar k/M$. (The standard Doppler limit $k_BT = \hbar\Gamma/3$ for an isotropic radiation pattern leads to a rms velocity of $12\hbar k/M$.) One clearly sees that during the evolution a narrower peak appears around the zero velocity with a width of $\sim 2\hbar k/M$. This peak is superimposed upon a much broader background. The reason that such a background remains present is because the con-

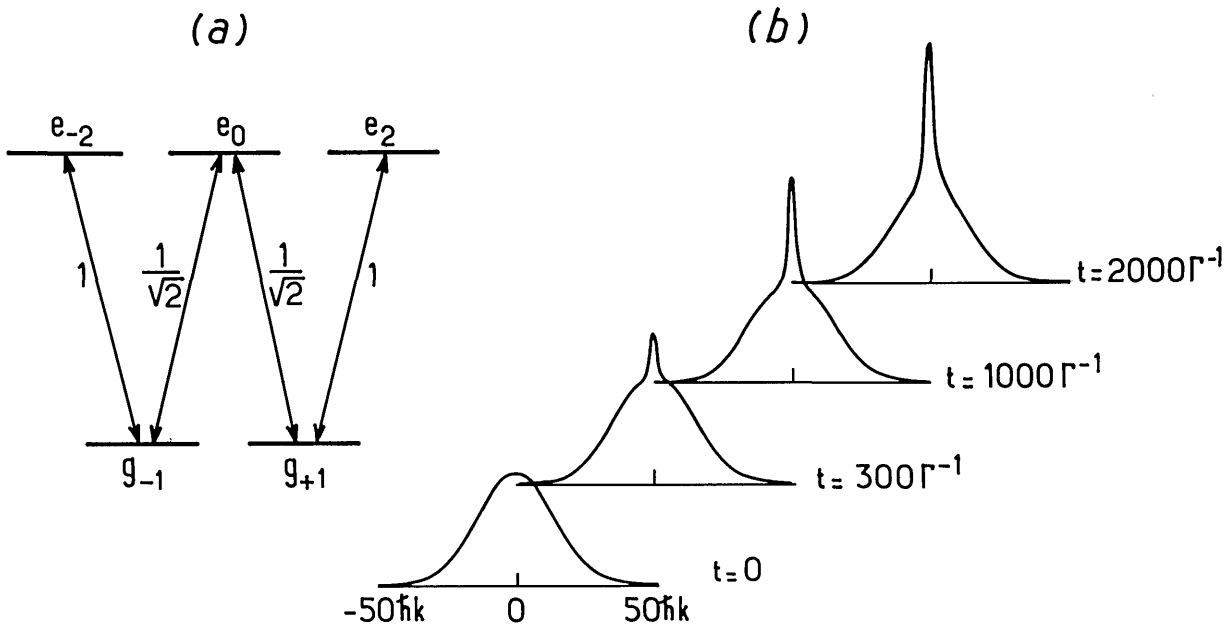

Fig. 9. (a) Fictitious W atom: This atom is the simplest atomic-level scheme leading to extra cooling in the $\sigma^+-\sigma^-$ configuration. (b) Time evolution of the atomic velocity distribution for a W transition ($\delta = -\Gamma$, $\Omega = 0.2\,\Gamma$, $\hbar\Gamma = 200\hbar^2k^2/M$ as for a sodium atom). The initial velocity distribution is chosen to be Gaussian with a rms width of 16 recoil velocities. The evolution is calculated via the generalized optical Bloch equations including recoil, which permit a full quantum treatment of atomic motion. During the evolution, the velocity distribution becomes non-Gaussian, with a very narrow peak (HWHM $\simeq$ 2 recoil velocities) superimposed upon a much broader background.

dition $kv \ll \Delta'$ for a linear force is not fulfilled for all velocity classes contributing to the equilibrium state. There are therefore still warmer atoms remaining in this equilibrium state. Note that such a non-Gaussian momentum distribution could be at the origin of the recent double-components velocity profiles measured in sodium molasses[8] (see also Ref. 30). We are currently working to improve this quantum treatment to take into account real atomic transitions ($J_g \leftrightarrow J_e = J_g + 1$), and we are studying the variations of the characteristics of the stationary state with laser power and detuning (see, for example, Ref. 31).

6. CONCLUSION

In conclusion, we have studied in this paper two new laser-cooling mechanisms that are based on laser polarization gradients and work at low laser power ($\Omega \ll \Gamma$). These two schemes are much more efficient than usual Doppler cooling, and they could be responsible for the anomalously low temperatures recently observed in 3-D molasses, where polarization gradients are certainly always present.

For simplicity, we limited our treatment to 1-D molasses and to transitions $J_g \leftrightarrow J_e = J_g + 1$. We clearly identified two types of polarization gradient; the first one corresponds to a gradient of ellipticity with fixed polarization axis (lin $\perp$ lin configuration) and the second to a pure rotation of the polarization axis with a fixed ellipticity ($\sigma^+-\sigma^-$ configuration). We showed that the cooling mechanisms are quite different in these two cases. In the first case, which works for $J_g \geqslant 1/2$, the light shifts of the ground-state sublevels are spatially modulated, and optical pumping between these states gives rise to a Sisyphus effect analogous to the one occurring in stimulated molasses but that works here at low intensity. In the second case, which works for $J_g \geqslant 1$, the cooling is due to an imbalance between the radiation pressures exerted by the two counterpropagating laser waves. This imbalance results from an ultrasensitive motion-induced population difference appearing among the ground-state sublevels.

These two new cooling mechanisms have a common characteristic: The friction coefficient α, i.e., the coefficient of proportionality between the friction force and the velocity v near $v = 0$, is independent of the laser power at low Rabi frequency. This must be contrasted with the result for usual Doppler cooling for which α is proportional to the laser power. On the contrary, the capture range of the cooling, i.e., the range of velocities over which the force is approximately linear, is now proportional to the laser power, whereas it is independent of this power for Doppler cooling. This can be summarized a follows:

$$\text{Doppler cooling} \begin{cases} \text{friction proportional to power} \\ \text{capture range independent of power} \end{cases},$$

$$\text{Polarization gradient cooling} \begin{cases} \text{friction independent of power} \\ \text{capture range proportional to power} \end{cases}$$

On the other hand, the momentum diffusion coefficient is in both cases proportional to the laser power, so that the steady-state temperature is proportional to the laser power for polarization gradient cooling, whereas, it is independent of this power for Doppler cooling. Note here that, although the two new mechanisms lead to a different variation with detuning for both the friction and the diffusion coefficients [compare Eqs. (4.26) and (4.35) with Eqs. (5.14) and (5.16)], the steady-state temperatures are actually found to be the same (in Ω^2/δ for large $|\delta|$), within a numerical factor [compare expression (4.37) with Eq. (5.18)].

The best way to check the theoretical predictions of this

paper experimentally is to investigate the velocity dependence of the friction force in 1-D molasses, for example, by studying the transverse collimation of an atomic beam crossing two counterpropagating laser waves with controllable polarizations. Actually, preliminary results have already been obtained on the $2^3S_1 \leftrightarrow 2^3P_2$ transition of helium.[32] They clearly show that cooling with orthogonal linear polarizations (i.e., with a polarization gradient) is more efficient than with parallel linear polarizations (no polarization gradient). Transverse temperatures below the Doppler limit T_D were measured in the lin $\perp$ lin configuration. For σ^+-σ^-, the residual kinetic energy remains of the order of the Doppler limit, but the velocity profiles are far from Gaussian. A full quantum treatment is certainly required in order to analyze them (see Subsection 5.D) because of the vicinity of the Doppler ($T_D = 23\mu K$) and recoil ($T_R = 4\mu K$) limits.

To extend our results to real 3-D molasses, one should first note that Doppler cooling is still present in these results (see, for example, Figs. 7 and 8). Therefore one takes advantage of both coolings: atoms with velocities of up to Γ/k are first Doppler-cooled and then reach lower temperatures by polarization gradient cooling. On the other hand, it does not seem easy to single out one of the two new cooling mechanisms since both types of polarization gradient are usually simultaneously present in a real 3-D experiment.

Finally, let us emphasize that the steady-state rms velocities that can be achieved in these new cooling schemes are very low, since they can approach the recoil velocity [see expressions (4.39) and (5.19)]. For such low velocities, a full quantum approach of both internal and external atomic degrees of freedom is required. The basis of such an approach and preliminary results are presented at the end of Section 5. We are currently extending this approach to more realistic situations, but these preliminary results already appear to be quite promising (see, for example, Ref. 31).

APPENDIX A: INTERNAL ATOMIC STATE IN THE MOVING ROTATING FRAME FOR THE σ^+-σ^- CONFIGURATION

In this appendix, we establish the expression of the new Hamiltonian that governs the atomic evolution in the moving rotating frame introduced in Subsection 3.B.2. We then determine the new ground-state energy sublevels in such a moving rotating frame (for a $J_g = 1$ ground state) and the expression of the steady-state density matrix in this energy basis.

Hamiltonian in the Moving Rotating Frame

In the laboratory frame and in the σ^+-σ^- laser configuration with $\mathcal{E}_0 = \mathcal{E}_0'$ [see Eq. (2.4)], the laser–atom coupling V is proportional to the component along ϵ_Y [given by Eq. (2.5b)] of the dipole moment operator $\mathbf{D}$. In the atomic-rest frame, we just replace z with vt, and we get from Eq. (2.5b)

$$V \sim \mathbf{D} \cdot \epsilon_y = D_x \sin kvt + D_y \cos kvt. \tag{A1}$$

The transformation to the moving rotating frame is then achieved by applying a unitary transformation

$$T(t) = \exp(-ikvtJ_z/\hbar). \tag{A2}$$

The only term of the initial Hamiltonian H that changes in such a transformation is V. Now, since $\mathbf{D}$ is a vector operator, its components satisfy the well-known commutation relations with J_z

$$[J_z, D_x] = i\hbar D_y, \qquad [J_z, D_y] = -i\hbar D_x, \tag{A3}$$

from which it is easy to show that

$$T(t)[D_x \sin kvt + D_y \cos kvt]T^+(t) = D_y. \tag{A4}$$

Thus it is clear that the transform of V by $T(t)$ describes the coupling of $\mathbf{D}$ with a laser field keeping a fixed polarization ϵ_y, which proves that $T(t)$ is the unitary operator associated with the transformation to the moving rotating frame.

The fact that $T(t)$ is time dependent introduces a new term, $i\hbar[dT(t)/dt]T^+(t)$, in addition to $T(t)H(t)T^+(t)$ in the Hamiltonian H' governing the time evolution in the new representation. According to Eq. (A2), we have

$$i\hbar\left[\frac{dT(t)}{dt}\right]T^+(t) = kvJ_z, \tag{A5}$$

which is nothing but Eqs. (3.13). To sum up, in the moving rotating frame, the atomic dynamics is due to coupling with a laser field with fixed polarization ϵ_y and to the inertial term [Eq. (A5)].

Ground-State Energy Sublevels in the Moving Rotating Frame

If, in a first step, we neglect the inertial term [Eq. (A5)], the energy sublevels in the ground state are the eigenstates $|g_m\rangle_y$ of J_y (see Subsection 3.B.1). These states can be easily expanded on the basis $\{|g_m\rangle_z\}$ of eigenstates of J_z. One gets

$$|g_{\pm1}\rangle_y = \pm\frac{1}{2}|g_{+1}\rangle_z + \frac{i}{\sqrt{2}}|g_0\rangle_z \mp \frac{1}{2}|g_{-1}\rangle_z, \tag{A6a}$$

$$|g_0\rangle_y = \frac{1}{\sqrt{2}}|g_{+1}\rangle_z + \frac{1}{\sqrt{2}}|g_{-1}\rangle_z. \tag{A6b}$$

From Eqs. (A6), one can then calculate the matrix elements of the inertial term [Eq. (A5)] between the $\{|g_m\rangle_y\}$ states that are necessary for a perturbative treatment of the effect of the term given by Eq. (A5) [see expression (3.14b)]. One finds that the only nonzero matrix elements of $V_{\text{rot}} = kvJ_z$ are

$${}_y\langle g_{+1}|V_{\text{rot}}|g_0\rangle_y = {}_y\langle g_0|V_{\text{rot}}|g_{+1}\rangle_y = \hbar kv/\sqrt{2}, \tag{A7a}$$

$${}_y\langle g_{-1}|V_{\text{rot}}|g_0\rangle_y = {}_y\langle g_0|V_{\text{rot}}|g_{-1}\rangle_y = -\hbar kv/\sqrt{2}. \tag{A7b}$$

Since V_{rot} has no diagonal elements in $|g_0\rangle_y$ and in the manifold $\{|g_{\pm1}\rangle_y\}$, the energy diagram in the ground state (see Fig. 6) is not changed to order 1 in V_{rot}. On the other hand, the wave functions are changed to order 1 and become

$$\overline{|g_{\pm1}\rangle_y} = |g_{\pm1}\rangle_y + |g_0\rangle_y \frac{{}_y\langle g_0|V_{\text{rot}}|g_{\pm1}\rangle_y}{\hbar(\Delta_1' - \Delta_0')}, \tag{A8a}$$

$$\overline{|g_0\rangle_y} = |g_0\rangle_y + |g_{+1}\rangle_y \frac{{}_y\langle g_{+1}|V_{\text{rot}}|g_0\rangle_y}{\hbar(\Delta_0' - \Delta_1')} + |g_{-1}\rangle_y \frac{{}_y\langle g_{-1}|V_{\text{rot}}|g_0\rangle_y}{\hbar(\Delta_0' - \Delta_1')}. \tag{A8b}$$

In Eq. (A8b), we used ${}_y\langle g_{+1}|V_{\rm rot}|g_{-1}\rangle_y = 0$. Inserting Eqs. (A7) into (A8) gives Eqs. (3.15) and (3.16).

Steady-State Density Matrix in the Energy Basis $\{|\overline{g_m}\rangle_y\}$

The terms describing optical pumping in the master equation are diagonal in the $\{|g_m\rangle_y\}$ basis. This is no longer the case in the $\{|\overline{g_m}\rangle_y\}$ basis. From Eqs. (3.15) and (3.16), one sees that there will be source terms of order 1 in kv/Δ' in the equation of motion of ${}_y\langle\overline{g_0}|\rho|\overline{g_{\pm1}}\rangle_y$ and of order 2 in kv/Δ' in the equations of motion of the populations ${}_y\langle\overline{g_m}|\rho|\overline{g_m}\rangle_y$ and of the coherence ${}_y\langle\overline{g_{+1}}|\rho|\overline{g_{-1}}\rangle_y$. The only nonzero matrix elements of ρ, to order 1 in kv/Δ', are thus ${}_y\langle\overline{g_0}|\rho|\overline{g_{\pm1}}\rangle_y$. On the other hand, since the evolution frequencies of these coherences are $\pm(\Delta_0' - \Delta_1')$, with a damping rate of the order of Γ', and since the optical-pumping source term is static (at frequency 0), the steady-state value of ${}_y\langle\overline{g_0}|\rho|\overline{g_{\pm1}}\rangle_y$ will be reduced by an extra nonsecular term of the order of Γ'/Δ'. Consequently, if we neglect all terms of order $(kv/\Delta')^2$, $(kv/\Delta')(\Gamma'/\Delta')$ or higher, the steady-state density matrix $\rho_{\rm st}$ is diagonal in the $\{|\overline{g_m}\rangle_y\}$ basis and has the same diagonal elements as those calculated in Subsection 3.B.1, which proves Eqs. (3.17).

APPENDIX B: $J_g = 1 \leftrightarrow J_e = 2$ TRANSITION IN THE σ^+-σ^- CONFIGURATION

The purpose of this appendix is to outline the calculations of the radiative force and of the momentum diffusion coefficient in the σ^+-σ^- configuration for the case of a $J_g = 1 \leftrightarrow J_e = 2$ transition. The calculation is done in the low-power limit ($\Omega \ll \Gamma$), so that excited-state populations remain small compared with ground-state populations. As explained at the beginning of Subsection 5.B, we calculate the force in the atomic reference frame, in which the atom–laser coupling is given by Eq. (5.1) and the radiative force by Eq. (5.3).

The first part of the calculation consists of calculating the optical coherences and the excited-state populations and coherences in terms of the ground-state populations and coherences. This gives first the expression of the force only in terms of ground-state variables (density-matrix elements in g), and second a closed system of five equations dealing only with ground-state variables. This system is finally solved numerically to get the value of the steady-state force.

Calculation of Optical Coherences

For simplicity, we introduce the following notation:

$$\bar\delta_\pm = \delta \pm kv + i\frac{\Gamma}{2},$$

$$\bar\delta_{3\pm} = \delta \pm 3kv + i\frac{\Gamma}{2}. \tag{B1}$$

The coherences $\tilde\rho(e_1, g_0)$ [Eq. (5.6)] and $\tilde\rho(e_{-1}, g_0)$ can then be written as

$$\tilde\rho(e_1, g_0) = \frac{\Omega}{2\sqrt{2}\bar\delta_-}\Pi_0,$$

$$\tilde\rho(e_{-1}, g_0) = \frac{\Omega}{2\sqrt{2}\bar\delta_+}\Pi_0. \tag{B2}$$

In a similar way, one calculates the other optical coherences

$$\tilde\rho(e_2, g_1) = \frac{\Omega}{2\bar\delta_-}\Pi_1, \qquad \tilde\rho(e_{-2}, g_{-1}) = \frac{\Omega}{2\bar\delta_+}\Pi_{-1},$$

$$\tilde\rho(e_0, g_1) = \frac{\Omega}{2\sqrt{6}\bar\delta_+}(\Pi_1 + C_r - iC_i),$$

$$\tilde\rho(e_0, g_{-1}) = \frac{\Omega}{2\sqrt{6}\bar\delta_-}(\Pi_{-1} + C_r + iC_i),$$

$$\tilde\rho(e_2, g_{-1}) = \frac{\Omega}{2\bar\delta_{3-}}(C_r + iC_i), \qquad \tilde\rho(e_{-2}, g_1) = \frac{\Omega}{2\bar\delta_{3+}}(C_r - iC_i) \tag{B3}$$

and the ones that can be deduced from Eqs. (B3) by complex conjugation. Note that several optical coherences, such as $\tilde\rho(e_0, g_0)$, have a zero steady-state value in this σ^+-σ^- configuration.

Putting the results [Eqs. (B2) and (B3)] into expression (5.3) for the force, one immediately gets Eq. (5.9), in which the force is expressed only in terms of Π_0, $\Pi_{\pm1}$, C_r, and C_i.

Calculation of Excited-State Populations and Coherences

We now calculate the expressions of excited-state populations and coherences in terms of ground-state variables. Take, for example, the evolution of $\rho(e_2, e_2)$, which is the population of the state e_2. The corresponding optical Bloch equation is

$$\dot\rho(e_2, e_2) = -\Gamma\rho(e_2, e_2) + i\frac{\Omega}{2}[\tilde\rho(e_2, g_1) - \tilde\rho(g_1, e_2)]. \tag{B4}$$

We take the steady-state value [$\dot\rho(e_2, e_2) = 0$], and we replace the optical coherences $\tilde\rho(e_2, g_1)$ and $\tilde\rho(g_1, e_2)$ by their expression in terms of ground-state variables [cf. Eqs. (B.3)]. This gives

$$\rho(e_2, e_2) = \frac{s_+}{2}\Pi_1, \tag{B5}$$

where s_+ is defined in Eq. (5.10).

We proceed in the same way for the other excited-state populations

$$\rho(e_1, e_1) = \frac{s_+}{4}\Pi_0 \qquad \rho(e_{-1}, e_{-1}) = \frac{s_-}{4}\Pi_0,$$

$$\rho(e_{-2}, e_{-2}) = \frac{s_-}{2}\Pi_{-1},$$

$$\rho(e_0, e_0) = \frac{s_-}{12}\Pi_1 + \frac{s_+}{12}\Pi_{-1} + \nu_1 C_r + \mu_1 C_i, \tag{B6}$$

where we have put

$$\mu_1 = [(\delta + kv)s_- - (\delta - kv)s_+]/6\Gamma,$$

$$\nu_1 = (s_+ + s_-)/12. \tag{B7}$$

The same procedure allows one to calculate excited-state coherences. We first define

$$\tilde\rho(e_1, e_{-1}) = \langle e_1|\rho|e_{-1}\rangle\exp(-2ikvt) \tag{B8}$$

(coherence between e_1 and e_{-1} in the moving rotating frame), which has the following equation of motion:

$$\dot{\tilde{\rho}}(e_1, e_{-1}) = -(\Gamma + 2ikv)\tilde{\rho}(e_1, e_{-1}) + \frac{i\Omega}{2\sqrt{2}}[\tilde{\rho}(e_1, g_0) - \tilde{\rho}(g_0, e_{-1})]. \quad \text{(B9)}$$

The steady-state value for $\tilde{\rho}(e_1, e_{-1})$ is then, using Eqs. (B2),

$$\tilde{\rho}(e_1, e_{-1}) = (\mu_2 + i\nu_2)\Pi_0, \quad \text{(B10)}$$

where we have put

$$\mu_2 = \frac{3\Gamma}{2}\frac{\nu_1\Gamma - 2\mu_1 kv}{\Gamma^2 + 4k^2v^2},$$
$$\nu_2 = -\frac{3\Gamma}{2}\frac{\mu_1\Gamma + 2\nu_1 kv}{\Gamma^2 + 4k^2v^2}. \quad \text{(B11)}$$

We also need for the following the quantity

$$\tilde{\rho}(e_2, e_0) + \tilde{\rho}(e_0, e_{-2}) = (\langle e_2|\rho|e_0\rangle + \langle e_0|\rho|e_{-2}\rangle)\exp(-2ikvt), \quad \text{(B12)}$$

which is found to be

$$\tilde{\rho}(e_2, e_0) + \tilde{\rho}(e_0, e_{-2}) = \sqrt{\frac{2}{3}}(\mu_2 + i\nu_2)(\Pi_1 + \Pi_{-1}) + (\mu_4 + i\nu_4)(C_r + iC_i), \quad \text{(B13a)}$$

with

$$\mu_4 = \sqrt{\frac{3}{2}}\frac{\Gamma}{\Gamma^2 + 4k^2v^2}[\Gamma(\nu_1 + \nu_3) - 2kv(\mu_1 + \mu_3)],$$
$$\nu_4 = -\sqrt{\frac{3}{2}}\frac{\Gamma}{\Gamma^2 + 4k^2v^2}[2kv(\nu_1 + \nu_3) + \Gamma(\mu_1 + \mu_3)] \quad \text{(B13b)}$$

and

$$\mu_3 = [(\delta + 3kv)s_{3-} - (\delta - 3kv)s_{3+}]/6\Gamma,$$
$$\nu_3 = (s_{3+} + s_{3-})/12. \quad \text{(B13c)}$$

Calculation of Ground-State Populations and Coherences

We now write the equations of motion of the ground-state populations. For example, we have for Π_1

$$\dot{\Pi}_1 = \Gamma\rho(e_2, e_2) + \frac{\Gamma}{2}\rho(e_1, e_1) + \frac{\Gamma}{6}\rho(e_0, e_0) + i\frac{\Omega}{2}[\tilde{\rho}(g_1, e_2) - \tilde{\rho}(e_2, g_1)] + i\frac{\Omega}{2\sqrt{6}}[\tilde{\rho}(g_1, e_0) - \tilde{\rho}(e_0, g_1)]. \quad \text{(B14)}$$

The first line describes how the state g_1 is fed by spontaneous emission from the three excited states e_2, e_1, e_0, and the second line describes absorption and stimulated-emission processes. In steady state, we can put $\dot{\Pi}_1 = 0$ and replace excited populations and optical coherences by their value in terms of ground-state variables. We obtain in this way

$$0 = -\frac{5}{6}s_-\Pi_1 + \frac{3}{2}s_+\Pi_0 + \frac{1}{6}s_+\Pi_{-1} + (2\nu_1 - s_-)C_r + 2\left(\mu_1 - \frac{\delta + kv}{\Gamma}s_-\right)C_i. \quad \text{(B15)}$$

In a similar way, we obtain from $\dot{\Pi}_{-1} = 0$

$$0 = \frac{1}{6}s_-\Pi_1 + \frac{3}{2}s_-\Pi_0 - \frac{5}{6}s_+\Pi_{-1} + (2\nu_1 - s_+)C_r + 2\left(\mu_1 + \frac{\delta - kv}{\Gamma}s_+\right)C_i. \quad \text{(B16)}$$

For the population Π_0, we just use

$$1 = \Pi_1 + \Pi_0 + \Pi_{-1} \quad \text{(B17)}$$

since excited-state populations are negligible at this order in Ω. We now write down the evolution equation of the ground-state coherence in the moving rotating frame:

$$\tilde{\rho}(g_1, g_{-1}) = \langle g_1|\rho|g_{-1}\rangle\exp(-2ikvt) = C_r + iC_i, \quad \text{(B18a)}$$

$$\dot{\tilde{\rho}}(g_1, g_{-1}) = -2ikv\tilde{\rho}(g_1, g_{-1}) + \frac{\Gamma}{2}\tilde{\rho}(e_1, e_{-1}) + \frac{\Gamma}{\sqrt{6}}[\tilde{\rho}(e_2, e_0) + \tilde{\rho}(e_0, e_{-2})] + i\frac{\Omega}{2\sqrt{6}}[\tilde{\rho}(g_1, e_0) - \tilde{\rho}(e_0, g_{-1})] + i\frac{\Omega}{2}[\tilde{\rho}(g_1, e_{-2}) - \tilde{\rho}(e_2, g_{-1})]. \quad \text{(B18b)}$$

We again replace the excited-state coherences and the optical coherences by their steady-state values. Taking the real part and the imaginary part of the equation $\dot{\tilde{\rho}}(g_1, g_{-1}) = 0$, we get

$$0 = \left(\mu_2 - \frac{s_-}{8}\right)\Pi_1 + \frac{3}{2}\mu_2\Pi_0 + \left(\mu_2 - \frac{s_+}{8}\right)\Pi_{-1} + \mu_5 C_r - \nu_5 C_i, \quad \text{(B19a)}$$

$$0 = \left(\nu_2 + s_-\frac{\delta + kv}{4\Gamma}\right)\Pi_1 + \frac{3}{2}\nu_2\Pi_0 + \left(\nu_2 - s_+\frac{\delta - kv}{4\Gamma}\right)\Pi_{-1} + \nu_5 C_r + \mu_5 C_i, \quad \text{(B19b)}$$

where

$$\mu_5 = \sqrt{\frac{3}{2}}\mu_4 - \frac{3}{2}\nu_1 - 9\nu_3, \quad \text{(B19c)}$$

$$\nu_5 = -\frac{6kv}{\Gamma} + \sqrt{\frac{3}{2}}\nu_4 + \frac{3}{2}\mu_1 + 9\mu_3. \quad \text{(B19d)}$$

The set formed by the five equations [Eqs. (B15)–(B19)] allows one to calculate numerically the five quantities $\Pi_{\pm 1}$, Π_0, C_r, and C_i for any value of the atomic velocity. Inserting the result into Eq. (5.9), one then gets the value of the radiative force for any atomic velocity in the low-power regime (see, e.g., Fig. 8).

In the very low-velocity domain ($kv \ll 1/T_p = \Gamma s_0$), the five previous equations can be simplified by neglecting all terms in kv/Γ and keeping only terms in $kv/\Gamma s_0$. We then put

$$s_+ = s_- = s_0, \quad \text{(B20)}$$

so that the previous set becomes

$$0 = -\frac{5}{6}\Pi_1 + \frac{3}{2}\Pi_0 + \frac{1}{6}\Pi_{-1} - \frac{2}{3}C_r - 2\frac{\delta}{\Gamma}C_i,$$

$$0 = \frac{1}{6}\Pi_1 + \frac{3}{2}\Pi_0 - \frac{5}{6}\Pi_{-1} - \frac{2}{3}C_r + 2\frac{\delta}{\Gamma}C_i,$$

$$1 = \Pi_1 + \Pi_0 + \Pi_{-1},$$

$$0 = \frac{1}{8}\Pi_1 + \frac{3}{8}\Pi_0 + \frac{1}{8}\Pi_{-1} - \frac{5}{4}C_r + \frac{6kv}{\Gamma s_0}C_i,$$

$$0 = \frac{\delta}{4\Gamma}\Pi_1 - \frac{\delta}{4\Gamma}\Pi_{-1} - \frac{6kv}{\Gamma s_0}C_r - \frac{5}{4}C_i. \tag{B21}$$

Then it is straightforward to check that the quantities given in Section 5 [Eqs. (5.11)] are indeed solutions of this simplified set.

On the other hand, for velocities such that $kv \gg 1/\tau_p$, the coherence between the two ground states g_1 and g_{-1} becomes negligible. One can then neglect C_r and C_i in the three equations [Eqs. (B16)–(B17)], which gives the simplified set

$$-5s_-\Pi_1 + 9s_+\Pi_0 + s_+\Pi_{-1} = 0,$$

$$s_-\Pi_1 + 9s_-\Pi_0 - 5s_+\Pi_{-1} = 0,$$

$$\Pi_1 + \Pi_0 + \Pi_{-1} = 1. \tag{B22}$$

The solution of this set is given in Eqs. (5.15). Inserting the corresponding values into expression (5.9) for the force, we recover the usual Doppler force, which has been plotted in dotted curves in Fig. 8.

Calculation of the Atomic Momentum Diffusion Coefficient

In order to calculate the momentum diffusion coefficient, we use a method introduced by Castin and Mølmer.[29] This method is well adapted to the present σ^+–σ^- laser configuration with a low laser power. It consists of writing down the generalized optical Bloch equations including recoil. Since we are interested here in the momentum diffusion coefficient, we take the limit of infinite atomic mass. This amounts to considering an atom with zero velocity but still exchanging momentum with the laser field, so that $\langle p^2\rangle$ increases linearly with time as $2Dt$. In order to get $d\langle p^2\rangle/dt$, we multiply the generalized optical Bloch equations (with $v = p/M = 0$) by p^2, and we integrate over p.

We start with the equation of motion for the population of $|g_0, p\rangle$, i.e., the atom in the ground state g_0 with momentum p:

$$\begin{aligned}\langle g_0, p|\dot{\rho}|g_0, p\rangle = {} & \frac{\Gamma}{2}\overline{\langle e_1, p|\rho|e_1, p\rangle} + \frac{2\Gamma}{3}\overline{\overline{\langle e_0, p|\rho|e_0, p\rangle}} \\ & + \frac{\Gamma}{2}\overline{\langle e_{-1}, p|\rho|e_{-1}, p\rangle} \\ & + \frac{i\Omega}{2\sqrt{2}}[\langle g_0, p|\rho|e_1, p+\hbar k\rangle \\ & + \langle g_0, p|\rho|e_{-1}, p-\hbar k\rangle]\exp(-i\omega_L t) + \text{c.c.}\end{aligned} \tag{B23}$$

The first two lines describe feeding by spontaneous emission, and the last two lines describe departure due to absorption. The single or double bar over $\langle e_i, p|\rho|e_i, p\rangle$ means an average over the momentum carried away by the fluorescence photon, either $\sigma_\pm$ polarized or π polarized:

$$\begin{aligned}\sigma_\pm\text{:}\quad \overline{\langle e_1, p|\rho|e_1, p\rangle} = {} & \int dp' \frac{3}{8\hbar k}\left(1 + \frac{p'^2}{\hbar^2 k^2}\right) \\ & \times \langle e_1, p+p'|\rho|e_1, p+p'\rangle, \\ \pi\text{:}\quad \overline{\overline{\langle e_0, p|\rho|e_0, p\rangle}} = {} & \int dp' \frac{3}{4\hbar k}\left(1 - \frac{p'^2}{\hbar^2 k^2}\right) \\ & \times \langle e_0, p+p'|\rho|e_0, p+p'\rangle.\end{aligned} \tag{B24}$$

We can in the same way rewrite all the other optical Bloch equations. This is done in detail in Refs. 18 and 19 for a $J_g = 0 \leftrightarrow J_e = 1$ transition or $J_g = 1 \leftrightarrow J_e = 0$ transition, so that we just give the main results here. First, owing to the conservation of angular momentum, the following family:

$$\{|e_m, p + m\hbar k\rangle; |g_n, p + n\hbar k\rangle\},$$

$$m = 0, \pm 1, \pm 2, \qquad n = 0, \pm 1$$

remains globally invariant in absorption and stimulated-emission processes. Transfers among families occur only via spontaneous-emission processes. Taking now the following notation:

$$\Pi_m(p) = \langle g_m, p + m\hbar k|\rho|g_m, p + m\hbar k\rangle, \qquad m = 0, \pm 1,$$

$$(C_r + iC_i)(p) = \langle g_1, p + \hbar k|\rho|g_{-1}, p - \hbar k\rangle, \tag{B25}$$

we can get a closed set of equations for these variables by elimination of the optical coherences and the excited-state populations and coherences. Here we just give the result of this elimination:

$$\begin{aligned}\dot{\Pi}_0(p) = {} & \frac{\Gamma s_0}{2}\left\{\frac{1}{9}\overline{\overline{\Pi_1(p)}} + \frac{1}{4}[\overline{\Pi_0(p-\hbar k)} + \overline{\Pi_0(p+\hbar k)}]\right. \\ & \left. - \Pi_0(p) + \frac{1}{9}\overline{\overline{\Pi_{-1}(p)}} + \frac{2}{9}C_r(p)\right\}, \\ \dot{\Pi}_1(p) = {} & \frac{\Gamma s_0}{2}\left\{\overline{\Pi_1(p-\hbar k)} + \frac{1}{36}\overline{\Pi_1(p+\hbar k)} - \frac{7}{6}\Pi_1(p)\right. \\ & + \frac{1}{4}\overline{\overline{\Pi_0(p)}} + \frac{1}{36}\overline{\Pi_{-1}(p+\hbar k)} + \frac{1}{18}\overline{C_r(p+\hbar k)} \\ & \left. - \frac{1}{6}C_r(p) - \frac{\delta}{3\Gamma}C_i(p)\right\}, \\ \dot{C}_i(p) = {} & \frac{\Gamma s_0}{2}\left\{\frac{\delta}{6\Gamma}[\Pi_1(p) - \Pi_{-1}(p)]\right. \\ & \left. + \frac{1}{6}[\overline{C_i(p-\hbar k)} + \overline{C_i(p+\hbar k)}] - \frac{7}{6}C_i(p)\right\}.\end{aligned} \tag{B26}$$

If one integrates these equations over p, one just recovers the stationary values deduced from Eqs. (5.11) for zero velocity. Now, multiplying these equations by p and integrating over p, we get

$$\langle pC_i\rangle = \int dp\, pC_i(p) = \frac{2\delta}{5\Gamma}\langle p\Pi_1\rangle,$$

$$\langle p\Pi_1\rangle = \frac{36}{17}\hbar k\frac{1}{1 + (4\delta^2/5\Gamma^2)} = -\langle p\Pi_{-1}\rangle; \tag{B27}$$

whereas for symmetry reasons one has

$$\langle p\Pi_0 \rangle = \langle pC_r \rangle = 0. \tag{B28}$$

We now multiply Eqs. (B26) by p^2 and integrate over p in order to get the rate of variation of $\langle p^2 \rangle$:

$$\frac{d}{dt}\langle p^2 \rangle = \frac{d}{dt}(\langle p^2\Pi_1 \rangle + \langle p^2\Pi_0 \rangle + \langle p^2\Pi_{-1} \rangle). \tag{B29}$$

Owing to symmetry around $p = 0$, one has $\langle p^2\dot{\Pi}_{-1} \rangle = \langle p^2\dot{\Pi}_1 \rangle$. After some calculations, we obtain from Eqs. (B26) and (B27)

$$\frac{d}{dt}\langle p^2 \rangle = \hbar^2 k^2 \Gamma s_0 \left\{ \frac{72}{17} \frac{1}{1 + (4\delta^2/5\Gamma^2)} + \frac{58}{85} \right\}, \tag{B30}$$

which represents twice the total momentum diffusion coefficient D. The two contributions D_1 and D_2 appearing in Eq. (5.16) can easily be deduced from this calculation. For example, D_1 represents the fluctuations of the momentum carried away by the fluorescence photons. If we replace in Eq. (B23) the kernel describing the spontaneous-emission pattern by just a $\delta(p')$ function, we cancel out this cause of diffusion. Then, repeating the same calculation again, we get an expression similar to Eq. (B30), where 58/85 is replaced by 8/17. This represents the contribution of the fluctuations of the difference among the numbers of photons absorbed in each wave (D_2 term). We then get D_1 by difference between D and D_2.

ACKNOWLEDGMENTS

The authors warmly thank all their colleagues from the Ecole Normale Supérieure laboratory and A. Aspect, E. Arimondo, Y. Castin, R. Kaiser, K. Mølmer, C. Salomon, and N. Vansteenkiste for many helpful discussions and remarks about this paper. They are also grateful to W. Phillips and his group for their comments on this work and communicating their experimental results previous to publication. Finally, they acknowledge stimulating discussions with S. Chu, H. Metcalf, and T. W. Hänsch last summer.

REFERENCES AND NOTES

1. T. W. Hänsch and A. Schawlow, Opt. Commun. **13,** 68 (1975).
2. D. Wineland and H. Dehmelt, Bull. Am. Phys. Soc. **20,** 637 (1975).
3. D. Wineland and W. Itano, Phys. Rev. A **20,** 1521 (1979); V. S. Letokhov and V. G. Minogin, Phys. Rev. **73,** 1 (1981).
4. S. Stenholm, Rev. Mod. Phys. **58,** 699 (1986).
5. S. Chu, L. Hollberg, J. E. Bjorkholm, A. Cable, and A. Ashkin, Phys. Rev. Lett. **55,** 48 (1985).
6. D. Sesko, C. G. Fan, and C. E. Wieman, J. Opt. Soc. Am. B **5,** 1225 (1988).
7. P. Lett, R. Watts, C. Westbrook, W. D. Phillips, P. Gould, and H. Metcalf, Phys. Rev. Lett. **61,** 169 (1988).
8. Y. Shevy, D. S. Weiss, and S. Chu, in *Proceedings of the Conference on Spin Polarized Quantum Systems*, S. Stringari, ed. (World Scientific, Singapore, 1989); Y. Shevy, D. S. Weiss, P. J. Ungar, and S. Chu, Phys. Rev. Lett. **62,** 1118 (1989).
9. J. Dalibard, C. Salomon, A. Aspect, E. Arimondo, R. Kaiser, N. Vansteenkiste, and C. Cohen-Tannoudji, in *Proceedings of the 11th Conference on Atomic Physics*, S. Harsche, J. C. Gay, and G. Grynberg, eds. (World Scientific, Singapore, 1989).
10. S. Chu, D. S. Weiss, Y. Shevy, and P. J. Ungar, in *Proceedings of the 11th Conference on Atomic Physics*, S. Harsche, J. C. Gay, and G. Grynberg, eds. (World Scientific, Singapore, 1989).
11. We restrict ourselves here to neutral atoms. Note that for trapped ions, mechanisms overcoming the Doppler limit were also proposed. They involve Raman two-photon processes: H. Dehmelt, G. Janik, and W. Nagourney, Bull. Am. Phys. Soc. **30,** 612 (1985); P. E. Toschek, Ann. Phys. (Paris) **10,** 761 (1985); M. Lindberg and J. Javanainen, J. Opt. Soc. Am. B **3,** 1008 (1986).
12. J. P. Gordon and A. Ashkin, Phys. Rev. A **21,** 1606 (1980).
13. J. Dalibard and C. Cohen-Tannoudji, J. Phys. B **18,** 1661 (1985).
14. Other consequences of long atomic pumping times are described in W. Gawlik, J. Kowalski, F. Träger, and M. Vollmer, J. Phys. B **20,** 997 (1987).
15. J. Javanainen and S. Stenholm, Appl. Phys. **21,** 35 (1980).
16. J. Dalibard and C. Cohen-Tannoudji, J. Opt. Soc. Am. B **2,** 1707 (1985).
17. A. Aspect, J. Dalibard, A. Heidmann, C. Salomon, and C. Cohen-Tannoudji, Phys. Rev. Lett. **57,** 1688 (1986).
18. A. Aspect, E. Arimondo, R. Kaiser, N. Vansteenkiste, and C. Cohen-Tannoudji, Phys. Rev. Lett. **61,** 826 (1988); J. Opt. Soc. Am. B **6,** 2112 (1989).
19. Y. Castin, H. Wallis, and J. Dalibard, J. Opt. Soc. Am. B **6,** 2046 (1989).
20. E. Arimondo, A. Bambini, and S. Stenholm, Phys. Rev. A **24,** 898 (1981).
21. J. Dalibard, S. Reynaud, and C. Cohen-Tannoudji, J. Phys. B **17,** 4577 (1984).
22. J.-C. Lehmann and C. Cohen-Tannoudji, C. R. Acad. Sci. **258,** 4463 (1964).
23. J. Dupont-Roc, S. Haroche, and C. Cohen-Tannoudji, Phys. Lett. **28A,** 638 (1969).
24. M. Lombardi, C. R. Acad. Sci. **265,** 191 (1967); J. Phys. **30,** 631 (1969).
25. C. Cohen-Tannoudji and J. Dupont-Roc, Opt. Commun. **1,** 184 (1969).
26. C. Cohen-Tannoudji, in *Frontiers in Laser Spectroscopy*, R. Balian, S. Haroche, and S. Liberman, eds. (North-Holland, Amsterdam, 1977).
27. We also reincluded in the definition of the excited states the phase factors $\exp(\pm i\pi/4)$ that appear when Eq. (2.7) is inserted into Eq. (4.1).
28. J. Dalibard, A. Heidmann, C. Salomon, A. Aspect, H. Metcalf, and C. Cohen-Tannoudji, in *Fundamentals of Quantum Optics II*, F. Ehlotzky, ed. (Springer-Verlag, Berlin 1987), p. 196.
29. K. Mølmer and Y. Castin, J. Phys. B (to be published).
30. D. S. Weiss, E. Riis, Y. Shevy, P. J. Ungar, and S. Chu, J. Opt. Soc. Am. B **6,** 2072 (1989).
31. Y. Castin, K. Mølmer, J. Dalibard, and C. Cohen-Tannoudji, in *Proceedings of the Ninth International Conference on Laser Spectroscopy*, M. Feld, A. Mooradian, and J. Thomas, eds. (Springer-Verlag, Berlin, 1989).
32. E. Arimondo, A. Aspect, R. Kaiser, C. Salomon, and N. Vansteenkiste, Laboratoire de Spectroscopic Hertzienne, Ecole Normale Supérieure, Université Paris VI, 24 Rue Lhomond, F-75231 Paris Cedex 05, France (personal communication).